Nuclear Wave Rotor Bi-Modal Cycle for In-Space Propulsion

Ryan Gosse *, Garrison Osborne †, Haris Mahmood ‡, Sarah K. Burrows §, Subrata Roy ¶, Justin Watson ‖, and Michael Tonks **
University of Florida, Gainesville, Florida, 32611, USA

Anthony J. Colozza ††
NASA Glenn Research Center, Cleveland, OH 44135, USA

Nuclear Thermal Propulsion (NTP) is currently identified as one of the preferred propulsion technologies for human missions throughout the solar system. The state-of-the-art NTP cycle is based on a solid core Nuclear Engine for Rocket Vehicle Application (NERVA) class technology that is envisioned to provide a specific impulse (I_{sp}) of 900 seconds doubling chemical rocket performance (450 seconds). Even with this impressive increase, the NTP I_{sp} still has issue providing adequate initial to final mass fractions for high ΔV missions. Nuclear Electric Propulsion (NEP) can provide extremely high I_{sp} (>10,000 seconds) but with only low thrust and limits on propulsion system mass to power ratio. The need for an electric power source also adds the issue of heat rejection in space where thermal energy conversion to electric is at best 30-40% under ideal conditions. A novel Wave Rotor (WR) topping cycle is proposed that promises to deliver thrust approaching NERVA class NTP propulsion, but with I_{sp} in the 1200-2000 second range. Integrated with a hybrid NEP mode, the duty cycle I_{sp} can further be increased (1800-4000 sec) with minimal additional dry mass. The bi-modal design enables a Fast Transit class human mission to Mars and has the potential to revolutionize the deep space exploration of our solar system.

I. Nomenclature

A	=	Area, m^2
C_P	=	Specific Heat Capacity at Constant Pressure, $\frac{kJ}{kgK}$
g	=	Earth Gravitational Acceleration, $\frac{m}{s^2}$
I_{SP}	=	Specific Impulse, s
k	=	Structural Coefficient
M_W	=	Molecular Weight $\frac{g}{mol}$
m	=	Mass, kg
$\dot{m}$	=	Mass Flow Rate, $\frac{kg}{s}$
PR	=	Pressure Ratio
PW	=	Power, kW
p	=	Pressure, kPa
R	=	Universal Gas Constant
SP	=	Specific Power $\frac{kW}{kg}$
T	=	Temperature, K
t	=	Time, s
v	=	Velocity $\frac{m}{s}$
V	=	Voltage, V
W	=	Work, kW
x	=	Distance, m
α	=	Specific Mass, $\frac{kg}{kW}$
γ	=	Specific Heat Ratio
γ_{acc}	=	Thrust Acceleration, $\frac{m}{s^2}$
ΔV	=	Velocity Change, $\frac{m}{s}$
ϵ	=	Emissivity
η	=	Efficiency
λ	=	Trajectory Characteristic Parameter
σ	=	Stefan-Boltzmann Constant

*Professor of Practice, Florida Applied Research in Engineering ryan.gosse@ufl.edu, AIAA Associate Fellow.
†Graduate Student, Department of Mechanical & Aerospace Engineering, g.osborne@ufl.edu
‡Undergraduate Student, Department of Mechanical & Aerospace Engineering, haris.mahmood@ufl.edu
§Graduate Student, Department of Mechanical & Aerospace Engineering, sarahburrows@ufl.edu
¶Professor, Department of Mechanical & Aerospace Engineering, roy@ufl.edu, AIAA Associate Fellow.
‖Associate Professor, Department of Materials Science & Engineering.
**Professor, Department of Materials Science & Engineering.
††Aerospace Engineer, Materials and Structures Division (LSM), Mail Stop 309-1.

Subscripts

avg	=	Average	Ma	=	Mars Arrival
Be	=	NEP Brayton Mode	o	=	Stagnation
Bt	=	NTP Brayton Mode	p	=	Propellant
$cable$	=	Power Distribution Cable	PL	=	Payload
$comp$	=	Compressor	PP	=	Power and Propulsion
e	=	Electric	rad	=	Radiator
Ed	=	Earth Departure	$reject$	=	Heat Rejection
et	=	Electric Thruster	S	=	Structure
$exit$	=	Exit State	th	=	Thermal
f	=	Final	tot	=	Total
Ht	=	Heliocentric Transfer	$trans$	=	Transit
i	=	Initial	$turb$	=	Turbine

II. Introduction

At a fundamental level, in-space Electric Propulsion (EP) is limited by the power cycle's ability to reject waste heat generated by its energy conversion process. This in turn produces a large heat load that requires an immensely heavy radiator, even at moderate thrust levels. Fig.1 shows the NASA Nuclear Electric Propulsion (NEP) - Chemical Propulsion (CP) Vehicle 1.2.[1] Note the large radiator area required for heat rejection of the 1.9 MW EP power system. Chemical and Nuclear Thermal Propulsion (NTP) designs, on the other hand, heat a working fluid and expel the hot gas with minimal heat transfer, reducing the cooling requirements to manageable levels at much higher levels of thrust.

The only way to reject heat in space is through radiation. If we assume the radiator is a black body, for discussion purposes, the power emitted is defined by,

$$PW_{\text{reject}} = A\sigma\epsilon(T^4_{\text{reject}} - T^4_{\text{background}}) \tag{1}$$

In interplanetary space, the background temperature is typically 3-200K. Brayton cycles are typically considered for the electric generation for high power systems using a solid nuclear core as used in the NASA NEP-CP vehicle 1.2 'reference vehicle. These systems typically provide a poor temperature to radiate waste heat. Focusing on the Brayton cycle turbine system to create electricity, higher rejection temperatures could be used but a fixed inlet temperature of the turbine means a lower output of power. To overcome this limitation, energy transfer processes with higher temperatures are required. In our work we explore the addition of wave rotor technology to overcome this limitation.

Fig. 1 NASA NEP-CP hybrid concept.

Another important aspect for nuclear based propulsion is the selection of the motive gas for the rocket. The selection is directly impacted by the desired specific impulse (Isp) and governed by the rocket equation as,

$$I_{\text{sp}} = \frac{1}{g}\sqrt{\frac{2\gamma}{(\gamma-1)}\frac{RT}{M_{\text{W}}}\left(1-\left(\frac{p_{exit}}{p_o}\right)\right)^{\left(\frac{\gamma-1}{\gamma}\right)}} \tag{2}$$

For a traditional chemical rocket utilizing hydrogen and oxygen, the combustion temperature is approximately 3420 K, the average molecular weight of the combusted gas is 13.8 g/mol, giving a maximum theoretical I_{sp} of 450 seconds with an optimized fuel rich mixing ratio. For an NTP solid core based on the Nuclear Engine for Rocket Vehicle Application (NERVA)[2] design, reactor material limits the gas heating to a 2,700-3,000 K rector exit temperature, but the rocket uses pure hydrogen that has a molecular weight of 2.016 g/mol. This gives the NTP a maximum I_{sp} of about twice that of the chemical rocket (900 sec). Reducing the molecular weight brings a significant performance increase. Fundamentally it would be ideal to reduce the molecular weight of the motive gas further. Fig.2 shows the phase change diagram for a pure hydrogen system. Over the pressure ranges relevant to rocket propulsion, complete atomization of hydrogen occurs in the range of 3150-5200 K. This is well beyond the service temperatures of solid core nuclear reactors. To reach these temperatures a liquid [3–7] or gas phase [8] reactor core would be required. Using an unsteady shock heating process, a wave rotor can theoretically reach liquid core performance while still using a nuclear reactor with a solid core. We have developed a unique cycle that leverages this capability.

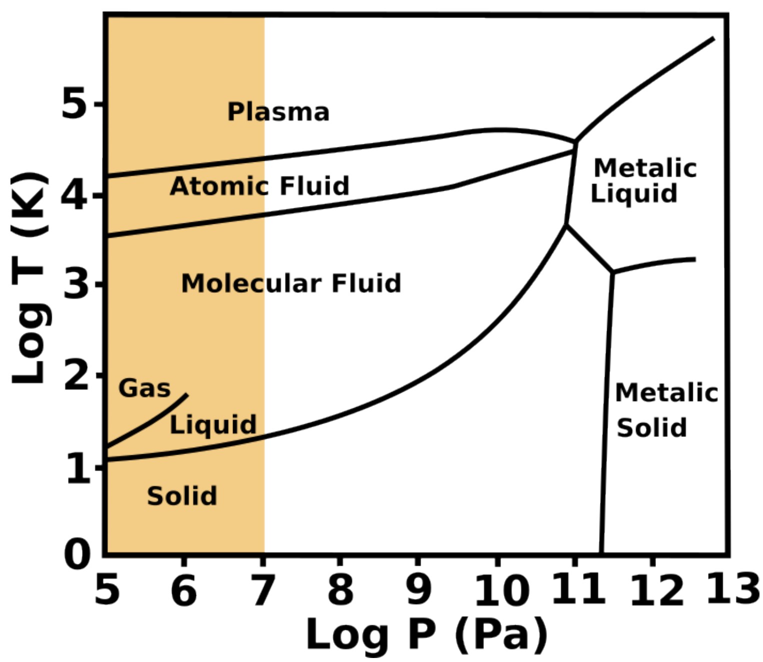

Fig. 2 Phase change diagram for hydrogen system. Yellow box represents practical pressure ranges of in-space rockets.

III. Incorporating Wave Rotor Technology

A wave rotor, wave-in-rotor, or dynamic-pressure exchanger (primarily in Europe) is a type of turbomachine in which energy is exchanged using shock waves onboard the rotor. A wave rotor can be configured with a variety of ports controlling the processing of the gas in the rotor channels. We chose to investigate a four-port wave rotor as shown in Fig.3. This configuration consists of a rotor, two end plates and a set of transition ducts. On the left side of the wave rotor, a High Pressure Driver Gas [HPDG] and Low Pressure Compressed Gas [LPCA] are directed through the ducts. Inflow ports are sized on the end plate to induce a harmonic injeciton of the two gasses. The rotor is made of a series of channels that operate as individual rotating shock tubes, compressing the LPCA gas with the HPDG gas. The technology has been used in combustion applications, refrigeration cycles and test gas compression/heating. To our knowlege, this system has never been explored for application as a topping cycle for an NTP rocket.[9–16]

Fig.4 shows a diagram of the compression and expansion waves in a four port wave rotor. In this figure the rotor from Fig.3 is cut and unwrapped from a cylinder to a flat plane with periodic boundaries. For visualization purposes, we

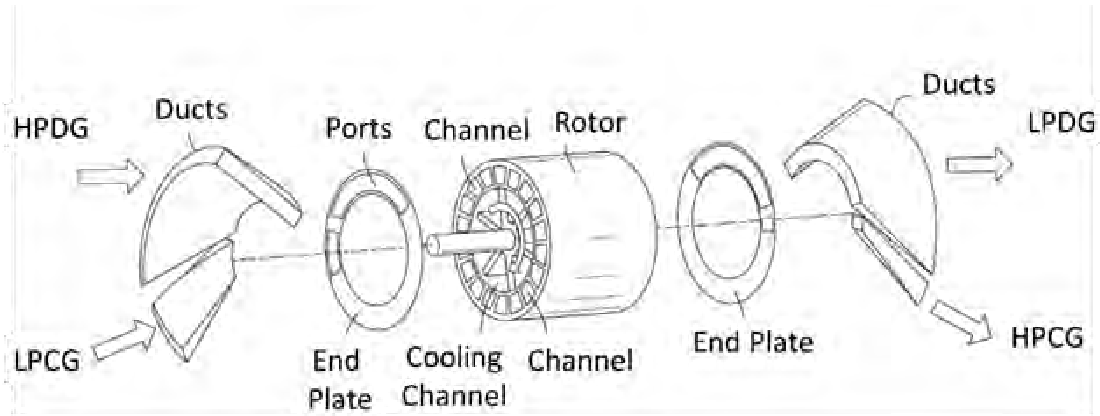

Fig. 3 Exploded view of a typical four port wave rotor. HPDG - High Pressure Driver Gas, LPDG - Low Pressure Driver Gas, LPCA - Low Pressure Compressed Gas, HPCG - High Pressure Compressed Gas.

assume that the rotor has a large number of channels making the volume of each infinitely small. This assumption allows for visualizing the fluid as a continuous domain. This visualization is similar to an x-t diagram for tracking the evolution of shock tubes. Inside the channels the blue color denotes the compressed gas and the gold color is the driver gas. At the interface of the two gases, a contact discontinuity exists. When the driver gas inlet port is opened, the contact discontinuity initiates a shock compression wave (red arrow). This wave travels at the convective velocity of the fluid plus the speed of sound. It therefore travels faster than the driver gas and compresses the compressed gas as it passes through it. When the shock hits the right wall of the channel (before the compressed gas outlet port opening) the shock reflects back further increasing the pressure of the compressed gas. Again the reflected shock travels faster than the velocity of fluid. Therefore, the compressed gas outlet port can be opened with out changing the nature of the compressing shock. Once the reflected shock reaches the left side of the channel, the driver gas inlet port is closed. An expansion wave is initiated by the end of injecting driver gas causing the driver gas velocity to go to zero. When the contact discontinuity reaches the compressed gas outlet port on the right, the port is closed. This traps the driver gas in a stagnate state. The driver gas outlet port is then opened to remove the driver gas. Another expansion wave is created that imparts the velocity to the gas for removal. When the expansion wave reaches the left side, the compressed gas inlet port is opened. The driver gas outlet port is then closed when the contact discontinuity between the two gases reaches the right side. When the driver gas outlet port is closed, another compression shock is initiated stagnating the compressed gas. When the shock reaches the left side of the channel, the compressed gas inlet port is closed. With the compressed gas stagnated, we reach a periodic boundary that enables the unsteady operation of the wave rotor.

A. Brayton Cycle with Topping Wave Rotor

Wilson and Paxson [17] along with Welch [18] conducted research on wave rotors for use as a topping cycle for jet engines. Their research found that the macroscopic balances of the volume-averaged thermodynamic properties in the rotor passage control volume can provide a simple system level analysis of performance. Fig.5 illustrates the use of a four port wave rotor in a Brayton cycle with a nuclear reactor core. We start at station 1.0 where low pressure working fluid enters the compressor. The air is compressed using a traditional axial or centrifugal compressor. The gas at station 2.0 enters the wave rotor and is further compressed by the hot gas entering at station 4.1. The gas then passes through station 3.0 at a higher pressure and travels to the nuclear reactor core (station 3.1). The nuclear reactor core heats the gas up to station 4.0. The hot gas then travels to 4.1 where it compresses the incoming low pressure gas from station 2.0. The gas then enters the turbine at 5.0 to extract the rest of the work from the gas. In between stations 1.0 and 6.0 the gas is cooled by a radiator to reject the excess enthalpy from the cycle. The radiator area sets the bottom temperature of the cycle and the nuclear reactor outlet temperature sets the top of the cycle.

Treating the wave rotor as a single control volume, we see that neglecting viscous effects, the work produced by the fluid entering and exiting the ports must be equal.

$$\dot{m}_{3.0-2.0} \int_{T_{2.0}}^{T_{3.0}} c_p(T)\, dT = \dot{m}_{4.1-5.0} \int_{T_{5.0}}^{T_{4.1}} c_p(T)\, dT \tag{3}$$

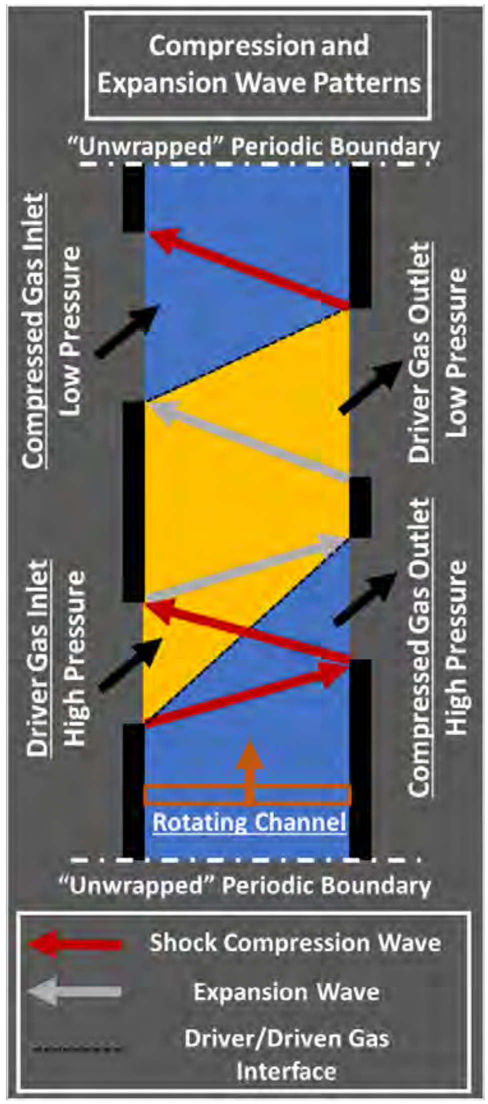

Fig. 4 Compression and expansion wave patterns in a four port wave rotor.

For this case the mass flow rate is the same throughout the system and can be neglected. Assuming we can model the compression and expansion of the gas as an overall polytropic process and that the heat capacity is only a function of gas temperatures by taking the average over the ports, the work between the inlet and outlet ports can be found by defining pressure ratios between the ports,

$$\dot{m}_{3.0-2.0}\int_{T_{2.0}}^{T_{3.0}} c_p(T)\,dT = \dot{m}_{3.0-2.0}\frac{c_{\mathrm{p,avg}}T_{2.0}}{\eta_{3.0-2.0}}[PR_{3.0-2.0}^{\frac{\gamma-1}{\gamma}} - 1] \tag{4}$$

$$\dot{m}_{4.1-5.0}\int_{T_{5.0}}^{T_{4.1}} c_p(T)\,dT = \dot{m}_{4.1-5.0}\,\eta_{4.1-5.0}\,c_{\mathrm{p,avg}}\,T_{4.1}\,[1-(\frac{PR_{2.0-5.0}}{PR_{3.0-2.0}})^{\frac{\gamma-1}{\gamma}}] \tag{5}$$

Where now the work can be computed using the inlet port temperatures and the pressure ratios. Equating the right hand side of Equations 4 and 5, the required pressure ratio from 2.0-5.0 can be computed if we assume the mass flow rate is the same through all ports as is the case for a nuclear powered Brayton cycle as opposed to one that involves a combustion process and the addition of fuel.

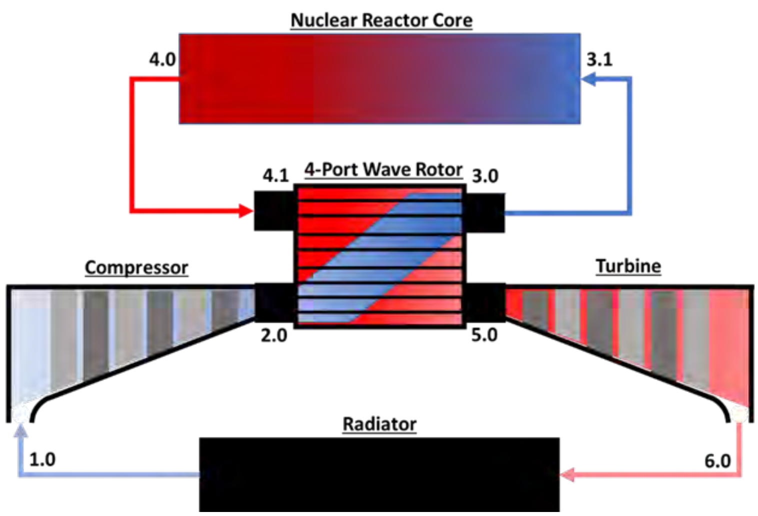

Fig. 5 Diagram of Brayton cycle with topping 4-port wave rotor.

$$PR_{2.0-5.0} = PR_{3.0-2.0}\left[\frac{1-\frac{(1-\eta_{4.1-5.0})}{\eta_{4.1-5.0}\,\eta_{3.0-2.0}}\frac{T_{2.0}}{T_{5.0}}\left[PR_{3.0-2.0}^{\frac{\gamma-1}{\gamma}}-1\right]}{1+\frac{1}{\eta_{3.0-2.0}}\frac{T_{2.0}}{T_{5.0}}\left[PR_{3.0-2.0}^{\frac{\gamma-1}{\gamma}}-1\right]}\right]^{\frac{\gamma}{\gamma-1}} \tag{6}$$

For completeness, the compressor power can be modeled using,

$$W_{\text{comp}} = \dot{m}_{1.0-2.0}\,c_{\text{p,avg}}\,\frac{T_{1.0}}{\eta_{1.0-2.0}}\left[PR_{1.0-2.0}^{\frac{\gamma-1}{\gamma}}-1\right] \tag{7}$$

And the turbine can be modeled using,

$$W_{\text{turb}} = \dot{m}_{5.0-6.0}\,c_{\text{p,avg}}\,\eta_{5.0-6.0}\,T_{5.0}\left[1-\left(\frac{1}{PR_{5.0-6.0}}\right)^{\frac{\gamma-1}{\gamma}}\right] \tag{8}$$

Balancing the work of the system, we see that the wave rotor can be viewed as removing the required compression from the compressor by using thermal energy from the reactor above the operating temperature of the turbine system. Due to the simple channel design and low rotation speeds compared to a traditional compressor, the wave rotor provides only a small addition of mass to the system compared to the significant increase in system net power. On a traditional Brayton cycle for space propulsion, the radiator rejects heat at average temperatures of at least 500 K for mass efficiency. One strategy of adding the wave rotor is pushing the rejection temperature up to a much higher value. Instead of adding extra power, it may be possible to significantly reduce the mass of the other propulsion system components resulting in a lower mass to power ratio. We will discuss this later as part of the bi-modal design.

B. Motive Gas Heating with Wave Rotor

NTP propulsion based on the NERVA concept is a simple expander cycle. The top of Fig.6 shows a detailed build up of the system based on recent work at NASA Glenn [19]. The bottom part of the figure shows the simplified system components that are relevant for our analysis. The cycle consists of a compressor that that takes the motive gas from a fuel tank and pressurizes the gas using turbomachinery. For the NERVA expander cycle, the turbomachinery is run by expanding a portion of the motive gas through a turbine and exiting the spacecraft out a separate small exhaust nozzle. The compressed gas then flows through the NTP reactor core where it is heated up to the desired temperature. The gas leaves the core and then is exhausted through the rocket nozzle. Again, the limiting factor maximizing I_{sp} is the maximum temperature of the NTP reactor core.

To increase the performance of the NTP mode, a wave rotor can be placed in between the NTP reactor core and the rocket nozzle as shown in Fig.7. In this configuration, the motive gas is compressed by a driver gas. Motive gas denotes

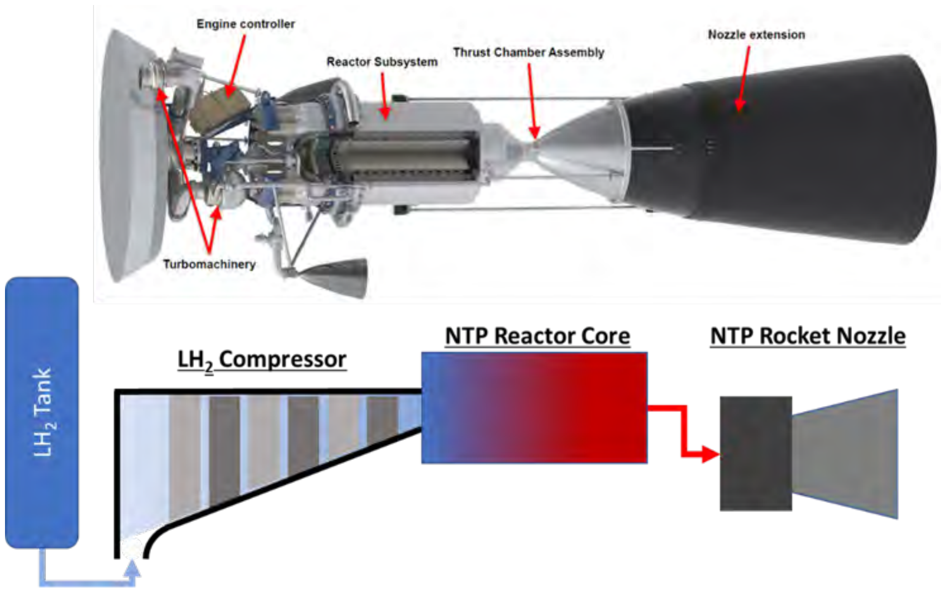

Fig. 6 NTP expander cycle. Detailed drawing from NASA Glenn (top) [19]. Simplified representation (bottom).

that gas is expelled by the rocket to produce motive force. Driver gas denotes the gas used to compress the motive gas (similar in reference to a driver gas in a shock tube). The driver gas in our case is also referred to as the Brayton cycle gas. The purpose of the driver gas is not to increase the pressure of the motive gas (as was the case for the Brayton cycle wave rotor), but to increase the motive gas temperature to values significantly beyond the traditional NTP NERVA design. Equations 4 and 5 can be recast into,

$$\dot{m}_{10.0-9.1} \int_{T_{9.1}}^{T_{10.0}} c_p(T)\, dT = \dot{m}_{10.0-9.1} \frac{c_{\text{p,avg}} T_{9.1}}{\eta_{10.0-9.1}} [PR_{10.0-9.1}^{\frac{\gamma-1}{\gamma}} - 1] \tag{9}$$

$$\dot{m}_{4.2-4.3} \int_{T_{4.2}}^{T_{4.3}} c_p(T)\, dT = \dot{m}_{4.2-4.3}\, \eta_{4.2-4.3}\, c_{\text{p,avg}}\, T_{4.2}\, [1 - (\frac{PR_{10.0-9.1}}{PR_{4.2-4.3}})^{\frac{\gamma-1}{\gamma}}] \tag{10}$$

Where the mass flow rate between the two do not have to be the same. This increases the number of unknowns, but we are now free to select the pressure ratio for both flow paths as an input parameter. The temperature inputs are also set by the reactor temperatures. Given a required thrust, the mass flow rate of 10.0-9.1 is fixed and we find the required mass flow rate for 4.2-4.3. We also point out that the temperature of the driver gas at 4.3 can be defined as the temperature required for the Brayton cycle wave rotor temperature at 4.1. Using this constraint, the pressure ratio of 4.2-4.3 can be found. Therefore, all the requirements for the NTP wave rotor can be defined.

C. Bi-modal Nuclear Core Operation

For the bi-modal core operation, the conditions for the NTP reactor core materials are extremely harsh. They must operate at temperatures ranging from 1000 K to nearly 3000 K with high temperature gradients and temperature cycling over time, as well as exposure to high-temperature flowing hydrogen. However, the propulsion cycles are short with a total irradiation time of only two days for a 45-day mission and less than 10 hours for a 65-day mission. Thus, they will not experience significant amounts of radiation damage or fission product buildup.

Three material systems are being considered for use in the fuel for NTP reactors: two composite fuel systems and one monolithic system. They all have strengths and weaknesses regarding use in NTP reactors. They are compared in Fig. 8, which shows the reactor exit temperature vs. projected endurance in hydrogen. Each is discussed in more detail, below.

In the ceramic-metal (cermet) composite concept, particles of a ceramic fuel are embedded in a metallic matrix. Early cermet concepts used a cermet fuel composed of uranium dioxide (UO_2) particles embedded in a tungsten (W) matrix [20]. Both of these materials has a melting temperature above 3000 K. However, this design required high enrichment to generate the desired temperatures due to the low uranium density of UO_2 and the high neutron

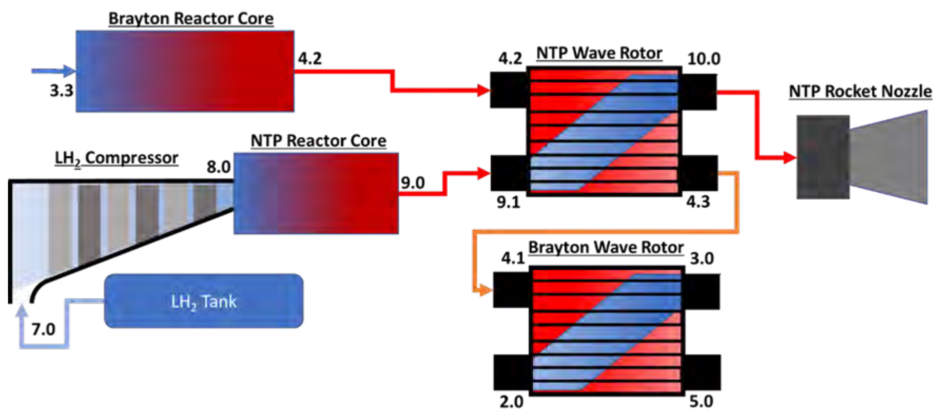

Fig. 7 NTP mode with wave rotor placed between reactor core and rocket nozzle. Brayton cycle components from Fig.5 are shown to describe where the power to heat the motive gas comes from.

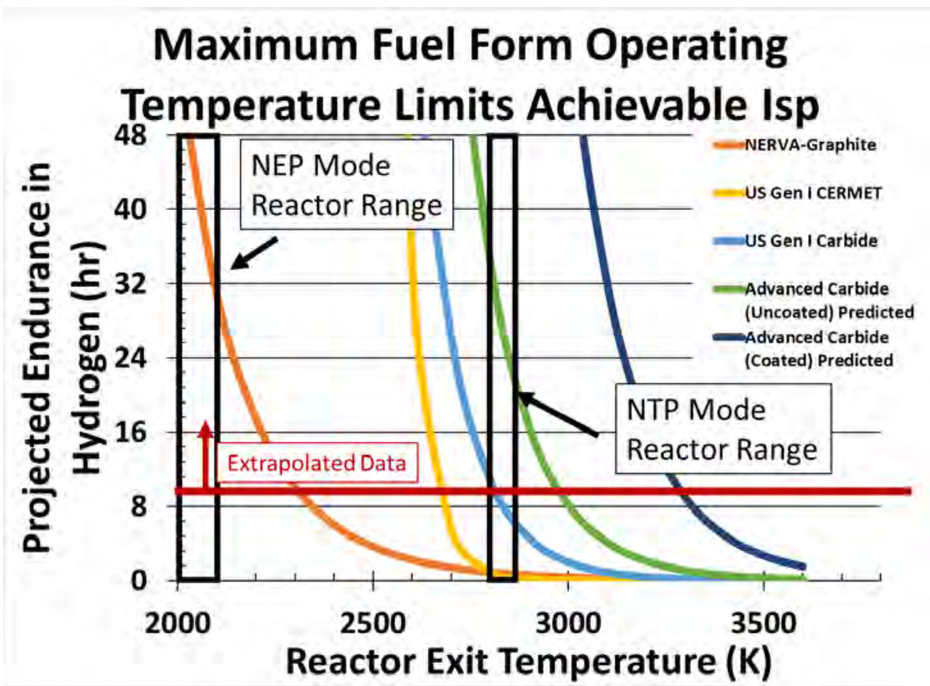

Fig. 8 Projected Endurance of nuclear core material technology vs. reactor exit temperature.

cross-section of W. A modern cermet concept uses uranium nitride (UN) particles embedded in a W-molybdenum (Mo) matrix. UN has a higher uranium density than UO_2 and still has a melting temperature above 3000 K. Increasing the Mo content in the W-Mo alloy decreases the neutron cross-section but also decreases the melting temperature. One major limitation of this concept is the decomposition reaction that occurs in UN fuel above 2120 K that is likely to result in fuel loss during operation [21].

In the ceramic-ceramic concept, ceramic particle fuel is embedded in a ceramic matrix [22]. The plan is to take advantage of the tristructural isotropic (TRISO) fuel particle technology in which a small fuel kernel is covered by various layers of carbonaceous materials. TRISO particles have demonstrated excellent performance for power reactors [23]. The fuel kernel could be made from either UN or a carbide fuel and zirconium carbide (ZrC) will be used in place of the SiC layer used in TRISO fuel. The fuel particles will be embedded in a ZrC or niobium carbide matrix [24]. ZrC has a melting temperature above 3000 K and a very low neutron cross-section. If UN is used as the fuel kernel, the decomposition reaction discussed in the previous paragraph would still be an issue. If uranium carbide (UC) is used as the fuel material, it would need to be mixed with refractory carbides such as ZrC to raise the melting temperature.

In the advanced carbide concept, a solid solution of ceramic materials is used as the fuel material [25]. Possibilities include a bicarbide (UC and ZrC) [26] and a tricarbide (UC, ZrC, and a third carbide such as tantalum, niobium, or W carbide) [27]. The melting temperature is raised above 3000 K by mixing with refactory carbides, and the cross-section is fairly low. The primary limitation of the advanced carbide concept is lack of data from high-temperature operation.

NEP reactor conditions are somewhat different than those for NTP. The temperatures would only reach up to around 2000 K, but the core may need to operate for much longer time. Due to the lower maximum temperature, some of the limitations of the fuel materials would not be present for an NEP core. With UN, the decomposition reaction would not have a significant effect, making that fuel a better option. Also, the operating temperatures would be below the melting temperature of UC so it would not need to be mixed with a refractory carbide. However, the longer operating times would add additional complications. There may be significant swelling and fission product buildup that could degrade the performance of the reactor.

A mixed mode reactor, that would operate for both the NTP and NEP propulsion modes, would pose the largest problem for the material performance in the core. The NTP modes would have the high temperature requirements and the total operating time would be the combined time of both NTP and NEP modes, meaning that even more swelling and fission product buildup could occur. The benefits to the design would be significant, but the actual design of the reactor materials would be more difficult.

Due to the harsh conditions within the NTP and NEP cores, it is difficult to solely use testing to ensure its performance. Modeling and simulation provide a useful tool for analyzing the thermomechanical behavior of the core materials during reactor operation, and reducing the required number of tests. Advanced simulation tools developed for modeling the fuel performance of power reactors are being taken advantage of to accelerate the development of models for propulsion reactors. The BISON fuel performance code [28] is being used to simulate the temperature throughout NTP cores [29, 30]. The mesoscale MARMOT tool is being used to determine effective properties of the core materials [29] and to investigate specific material behaviors such as fuel loss [21]. Such methods should be applied to investigate the reactor designs for NTP and NEP cores, as well as for mixed mode cores.

IV. Wave Rotor Enhanced Nuclear (WREN) Propulsion Bi-modal Cycle

A. Modeled Propulsion Subsystems Overview

The generalized concept for the bi-modal design is show in Fig.9. The main focus of this work is the improvement in NTP performance. In this regard, there are two main lines of fluid flow. One is the motive gas line that is expelled from the NTP rocket nozzle to produce thrust and the other is the driver gas line as part of a Brayton cycle to supply compression work on the motive gas. For this work we chose to use hydrogen gas for both the motive and Brayton cycle gas. Depending on mission requirements, using different gas species for the motive and Brayton cycle gas may lead to more optimal designs.

The motive gas is compressed by a turbopump and sent to a recuporator, providing the reservoir temperature for cooling the driver gas in the Brayton cycle loop. Afterwards, the motive gas is sent to the NTP core (nuclear reactor) for heating. It then goes to the wave rotor for further heating and then expelled out the nozzle.

The driver gas goes through a Brayton cycle similar to Fig.5, but with an additional compressor to supply the required pressure increase for the NTP Wave Rotor compression process. This places an additional compression load on the Brayton cycle when operating in the NTP mode. A series of divert valves change the flow of the system between NTP and NEP modes. In this concept, the second compressor is bypassed when the NTP Wave Rotor is not in use. Fig.9 does not show the divert valves. Instead, two gas loops are shown to denote the Brayton cycle gas flow during the NTP and NEP modes. The NTP mode loop is denoted by the subscript Bt and the NEP mode loop is denoted by the subscript Be. It can be seen that the main difference between the two loops is the second compressor and NTP Wave Rotor is bypassed when in NEP mode. Additionally, we note that Radiator 2 is shown as Radiator 2.1 and 2.2. This is to denote how the power is rejected differently between the two modes. A series of control valves couple the radiator to the respective gas loop locations. During NEP mode, heat rejection of the alternator and Power Management and Distribution (PMAD) system is added to the rejection system. Therefore the heat load on Radiator 2 is different between NTP and NEP modes. When in NEP mode, the Alternator is engaged to extract excess power into electricity. This power is conditioned by the PMAD system and sent to the NEP thrusters.

Again, for this concept the wave rotor cycle operates at a temperature significantly above the limits of the in-space turbine technology. The Brayton nuclear reactor core operates at two temperature points. One at extremely high core temperature, but for a relatively short period during operation of the NTP mode. The second at a more moderate temperature, but still relatively high core temperature compared to other NEP modes. As discussed in Section III.C, it is not clear if a single core or multi-core reactor is required.

In order to model the system as a whole, an object oriented programming (OOP) MATLAB program was developed. Each subsystem is modeled as on independent object allowing the application of different constraints on the propulsion system for optimization. These object classes were established as either inheriting or being composed of other classes dependent on modeling needs. For example, all of the engine sub-components which contain some sort of gas flow (i.e. Wave Rotor, Turbine, etc.) are given the thermochemical qualities of the gas class to determine work processes. The gas class contains 9-coefficient curve fit functions for the specific heat (C_p), enthalpy, and ratio of specific heats (γ) of gas species based on empirical data derived from the NASA Chemical Equilibrium and Applications (CEA) code [31][32]. These curve fits are functions of temperature and are therefore thermally perfect. This is useful for our model because both the driver and motive gas are not chemically reacting except for hydrogen dissociation in the NTP Wave Rotor, all heat and work exchanges are assumed volume-averaged, ideal systems, and the high number of coefficients ensure high result fidelity.

Again in this work, we focus on a practical improvement to the NTP system by maximizing the I_{sp} for a given thrust. This was conducted with out regard to mission requirements except for improving the NEP system mass to power ratio defined as the parameter α in section V.B. In our work we define alpha as the power of the propulsion cycle divided by all of the systems shown in Fig.9. Compared to a pure NEP mode, this makes our NEP alpha larger. The following sections go over the assumptions made for each of the subsystems.

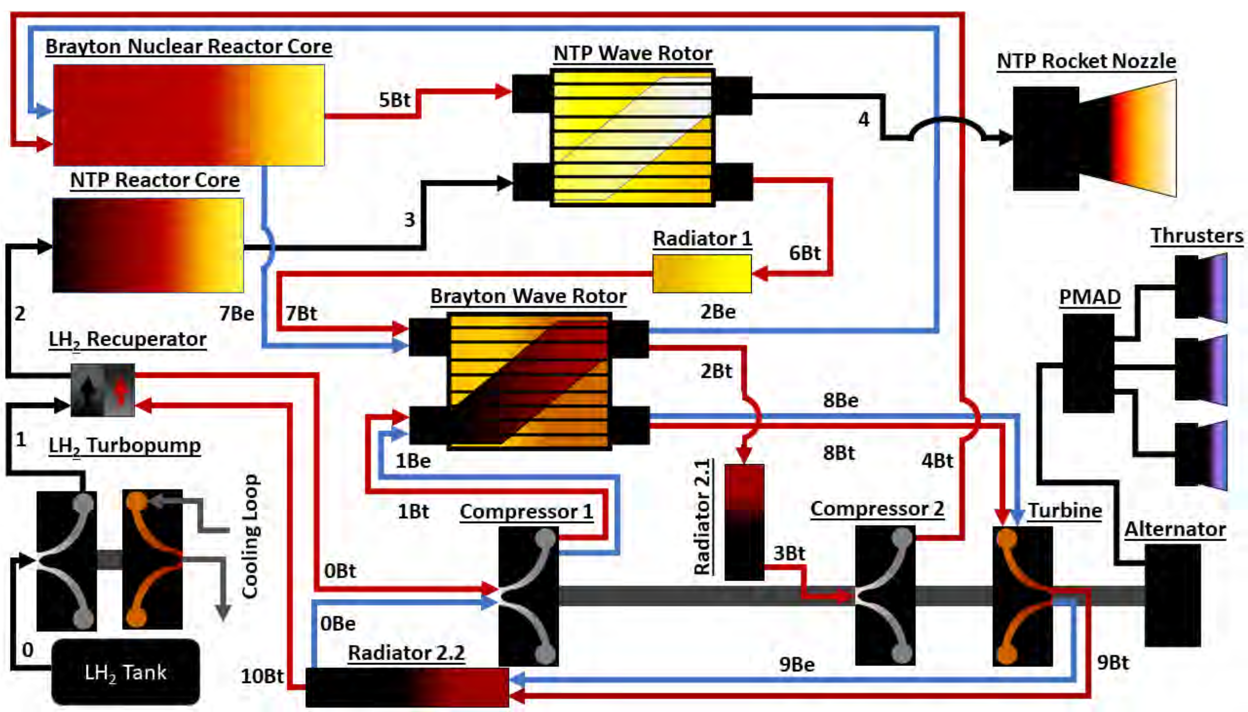

Fig. 9 Preliminary system concept for bi-modal NTP/NEP propulsion system with wave rotor topping cycle. Sub-components are colored in visible black body radiation spectrum to give qualitative description of the gas temperature. Different cycle and mode lines are indicated by colored arrows: black for the motive gas cycle during NTP mode; red for Brayton cycle during NTP mode; blue for Brayton cycle during NEP mode.

1. Wave Rotors

As was outlined in section III.A, each wave rotor within this system concept can be modeled using simple macroscopic balances of the volume-averaged thermodynamic properties within the rotor passages. Again in this concept, both the driver gas and compression gas in the wave rotors are hydrogen. The primary motivation for this choice is the lack of fidelity to capture mixing of the motive and driver gas inside the wave rotor using the macro-scale model. Note that the shock processes in the wave rotor are initiated by the gas contact discontinuities. The process is inherently driven by inviscid forces, but the viscous diffusion forces of the high gradient regions will produce a small amount of mixing. Additionally, the opening and closing of port doors is not instantaneous. If the open/close process is slow, mixing may also occur. Such analysis requires the use of computational fluid dynamics modeling. These losses are included in wave rotor efficiency parameters found in equations 4 and 5. For this model, all efficiencies were fixed at 80 percent, both for the compression and expansion process.

The mass of the wave rotor is negligible compared to the whole system. However as a demonstration of how tenuous it's mass is compared to its power conversion contribution, a simple solid cylinder of high density carbon carbon composite (C/C) was included to represent the rotor, its housing, and motor. Because the wave rotor does not directly apply work to the gas, very little power is required for rotation, and so the motors are quite small. With a minimum density of 1.8 g/cm^3, the wave rotor's of the system would barely constitute a fraction of a percent of the engine mass given current estimated sizes of less than a 0.5 meters in height and diameter.

The choice of high density C/C was for the composite's ability to retain its mechanical properties for temperatures at or above 2800K. Though exposure to hydrogen will require additional protective surface coatings. The wave rotors uniquely unsteady flow environment could theoretically allow for exceptionally high gas temperatures, resulting in a service temperature closer to the exit temperature of the driver gas. This is because walls of the rotor channels are constantly exposed to hot and cold flows in approximately equal periods over a full rotation [33]. In addition to the flow timing analysis, a focus on thermal loads will be necessary in order to determine points of active cooling if passive cooling does not suffice.

2. LH_2 Turbopump

The work of the LH_2 compressor was found using a scaling parameter for the Space Shuttle main engine (SSME) LH_2 turbopump as conducted in similar NTP studies [34]. Previous work on turbopump designs by NASA was also available [35]. For their NERVA derived design with a thrust of 111.2 kN, the mass of the turbopump was approximately 100 kg. The power of the pump was functionally coupled with the NTP wave rotor and its compression process (ports 3 to 4). This design makes up for the pressure losses of the motive hydrogen when it passes over the recuperator and the NTP reactor core, allowing the gas to attain the required pressure balance.

The turbine would derive power from a regenerative cooling loop similar to the liquid rocket cycle of the SSME. This line of hydrogen would be used for active cooling of the reactor cores, the NTP rocket nozzle, NTP Wave Rotor, etc. We assume this cooling would be conducted at station 2 after cooling the Brayton gas loop and hence the grey open loop arrows in Fig.9 to simply the description for this work. Details of the cooling lines will also be reserved for future research, as this system overview is only concerned with the engine dry mass. However, future research into a valved tap-off cycle has been considered where the tapped hydrogen could be bypassed from the turbopump into the NTP rocket nozzle to induce some throttleability during the NTP phase.

3. Recuperator

A recuperator is included to provide additional cooling to the Brayton cycle when operating in NTP mode. The lightweight mass model is adapted from a micro shell-and-tube model for use in turbo-Brayton cryocoolers of air and space vehicles [36]. Although a recuperator is able to operate in the temperature and pressure ranges we introduce for the exchanging lines with a high efficiency, it should be noted that an improved model will be necessary as Zagarola and McCormick [36] utilized a recuperator meant for monatomic noble gases. Regardless, this heat exchanger is assumed to extremely light; comparable to the wave rotors in mass.

The recuperator will not be in operation during the NEP mode because liquid hydrogen is no longer being fed from the LH_2 tank. For this reason, balancing the cycle gasses surrounding the Brayton Wave Rotor will be met by routing the driver gas through both radiator 2.2 and 2.1 to meet cooling needs. This will be done by bypassing station 10Bt and 0Bt surrounding the recuperator. Station 0Be will be the new driver gas line which passes over radiator 2.1 following radiator 2.2 (note: this line switch is not shown in fig.9 for simplicity). Estimates indicate that a little under half of radiator 2.1 will be devoted to driver gas cooling during NEP mode, the other half will provide cooling to the Alternator and PMAD.

4. Turbine

The purpose of previously published mass-power scaling factors is motivated by the ease of preliminary estimates of system mass contribution. The change in enthalpy of the driver gas as it passes over the turbine determines the work done given its mass flow rate. As such, an isentropic expansion of a thermally perfect gas model is used to determine the work output of the turbine based on equation 8. The turbine in this model is assumed to have an efficiency of 85% The mass scaling parameter is the average specific mass of turbines outlined in previous space nuclear power systems studies [37]. This parameter was originally published in 1987, thus it can be inferred that our model overestimates the actual weight of the turbine since turbomachinery technology and materials have improved since then. The same assumption goes for the compressors and alternator. For example SiC/SiC Ceramic Matrix Composites (CMC) have a density that is a third of superalloys[38]. Recent work has also referenced the values from Walter [39][40].

The inlet temperature of a turbine is set to 1650 K based on material limit estimations. Current in-space turbines operate at 1200 K for He-Xe gases and 973 K for CO2[41]. Work by Duchek[42] suggested a turbine inlet temperature of 1400 K to be a key performance parameter. The in-space Brayton cycle study by Morrison[40] suggested that an turbine inlet temperature of 1800 K would be feasible based on advanced materials and film cooling. NASA Glenn has focused on a 1750 K SiC/SiC Ceramic Matrix Composite (CMC) for aviation turbine use[43], but with a target strength of 20 ksi for only 300 hours. Recent work supported by NASA Glenn [44] showed a consistent cycle life for SiC/SiC CMC blade material between 1500 F (1088 K) and 2400 F (1588 K) as part of their high cycle fatigue test program. This technology used in conjunction with a thermal barrier coating could achieve an operational temperature of 1650 K. Hence we use this value as the upper limit for the WREN turbine technology.

5. Compressor

Similar to the Turbine, the two compressors are modeled based on an average mass-power scaling [37] and subject a thermally perfect driver gas to isentropic compression, i.e. eq. 7. The compressors in this model are assumed to have an efficiency of 85%. The purpose of Compressor 1 and Compressor 2 are quite different from one-another despite sharing the main drive shaft. Compressor 2 serves to balance the Brayton loop when it is coupled with the NTP Wave Rotor during NTP mode, while Compressor 1 functions as a typical Brayton cycle compressor for both NTP and NEP mode. During the NEP mode Compressor 2 will be shut off and the driver gas will bypass it.

The mode change from NTP to NEP has introduced some notable challenges in terms of pressure and temperature balances. A primary requirement for the bi-modal system is to maintain the same operating conditions of the Brayton Wave Rotor for both modes. This is because of the extremely limited range of conditions that the wave rotor can properly operate. The state-of-the-art wave rotor technology still uses a fixed port timing fixing port conditions. Therefore, the compressor system is designed having two-stages. It must also be noted that the wave rotor compression process is set by the speeds of the compression and expansion waves inside the channel. Cooler gas temperatures during the NEP mode, may required an adaptive port timing system or the addition of a third wave rotor to handle the different port conditions. We currently ignore such issues in this systems level study. To better understand this issue, detailed computational fluid dynamics modeling of the wave rotor will be required.

6. Radiator

Radiators are used to reject the excess heat from each of the main systems to space. The radiators are sized based on energy balance approach for rejecting excess heat to the surroundings. Heat inputs and view factors to surrounding components of an environmental body such as the sun and planets are required to be taken into account in this energy balance approach. For a Earth to Mars mission, the Earth environment during NTP mode operation is considered the worst case scenario. The required radiator area is determined by the thermal power that needs to be rejected. For the WREN propulsion system, two main radiators are employed. Radiator 1 is used to moderate the temperature between the two wave rotors. It serves to limit the temperature of the Brayton cycle gas at the turbine inlet. Radiator 2 is the first stage of heat rejection for the two compressors. Fig. 9 shows a Radiator 2.1 and Radiator 2.2 subsystems. This is to denote the different heat rejection requirements of the two modes and the interface to Radiator 2. During NTP mode, Radiator 2.1 acts as an inter-cooler between the Brayton Wave Rotor and Compressor 2. In NEP mode, Compressor 2 is by-passed and additional heat can be rejected by Radiator 2.2. This radiator is then used to cool the alternator and PMAD systems. Any additional area is given to Radiator 2.1 to allow for reducing Compressor 1 inlet temperature.

We used the same design methodology as for the NASA Compass study of the NEP-CP 1.2 reference vehicle [1]. The design uses a pump loop cooling system due to the high heat loads. The pump loop system is broken into segments and is controlled by a series of valves and sensors. H_2 gas mixing from Radiator 2.1 and 2.2 can then be controlled. Leakage of H_2 during operation was not considered due to the expected short transit times compared to the total H_2 required for NTP motive gas. It was found that the high speed of sound of H_2 provided improved heat transport properties compared to HeXe gas typically used for the Brayton cycle. A range of expected power loads for the NTP and

NEP modes was approximated and used to create three radiator designs. The resulting radiator mass and areas were fit to curves based on the average radiator temperature.

$$m_{rad} = 8.26815 \cdot 10^{13} \cdot T_{avg}^{-4.025} \cdot PW_{reject} \tag{11}$$

$$A_{rad} = 2.756 \cdot 10^{13} \cdot T_{avg}^{-4.024} \cdot PW_{reject} \tag{12}$$

Radiator 1 operates at extremely high temperatures. We assumed that it would be made out of a series of graphite or ceramic tubing. Control of heat rejection would be conducted by a series of rotating insulating covers to control the heat rejection area. Additional radiator panels are required for the PMAD system. These were considered as included in the mass budget of this subsystem. Other heat rejection requirements for the fuel tanks, crewed module, ect. do not use Radiator 1 or 2 and are included in their respective systems.

There are also potentially lighter mass radiator system technologies such as reported by Tombuilian [45] that is based on carbon fiber fabric. Incorporating such technology could potentially double the specific heat rejection (W/kg) of the individual heat pipes leading to a significant reduction in the radiator mass. For this study we chose the higher Technology Readiness Level (TRL) materials to show the benefits of adding a wave rotor vs. NASA's current baseline systems.

7. Nuclear Reactor

As described in section III.C, the optimal design of a nuclear core for use in the WREN system has not been explored. We decided to use an exit temperature of 2850 K for the nuclear core when in NTP mode. This is close to the desire by NASA for a 900 second specific impulse $I_{\rm sp}$ traditional NTP design [46]. Refering to Fig. 8 higher temperatures could be used, but we expect the NTP mode to operate longer due the extra propulsion mass vs. available thrust of the bi-modal system. The NEP reactor exit core requirements will be much lower due to our desire to have the same gas mass flow rate through the Brayton cycle for both modes. This assumption is applied with the desire to maximize the electric power of the NEP mode. Fig. 9 shows two reactor cores. This does not preclude that individual cores are required but to capture the worst case scenario of the different thermal and power load requirements between the needs of the Brayton cycle loop and the heating of the motive gas. The total power requirement of each mode is used to estimate the required reactor mass. To estimate the mass requirements of the core, we relied on NTP core designs with low power [47][48]. These designs resulted in mass to thermal power ratios ranging from 0.006 to 0.01 kg/kW_{th}. For conservatism we chose a value of 0.1 kg/kW_{th}. For the gas flowing through the reactor core, we assumed a pressure loss of 2%.

8. Nuclear Reactor Shield

Referring to the NEP-CP 1.2 reference vehicle study [1], the design of the nuclear core reactor shield is a complicated process. Modeling and simulation code is used to predict the radiation environment in the shadow of the shield with respect to the nuclear reactor core. For our level of detail we relied on past work [49] to develop a scaling parameter. They suggested a human at most should receive a dose of 5 rem for a mission. A relationship between required shield mass and crew dosage was given for a 75,000 lbf NERVA-derivative engine. This power is in the same class as the WREN system. We decided to lower the dosage requirement to 2 rem. This resulted in a mass to thermal power ratio of 0.008 kg/kW_{th}.

9. Alternator

The power of an alternator is directly coupled with the output work of a turbine, i.e. a turboalterantor. Similar to the turbine and compressors, a mass-power scaling is used (0.2 kg/kW)[37]. The operational efficiency is assumed to be 97% [50][51]. The maximum continuous operating temperature of the alternator for this design is 500 K [52]. For an alternator processing 50 MW of input work, the power rejection requirements would be 1.5 MW. If it operates continuously at 450K, it will require approximately 1600 m^2 of Radiator 2 for cooling.

10. Power Management and Distribution (PMAD)

After work is extracted from the Brayton turboset by the alternator in NEP mode, the electric power must be correctly conditioned for distribution to the electric thrusters. The largest contribution to mass is the direct current (DC) to DC converter. The Kilowatt project for distributing power on the Moon was found to be one of the most recent works providing data for actual systems[53]. The largest units produced for extraterrestrial use reach 200 kW. A linear relationship was given to compute the specific power (kW/kg).

$$SP_{PMAD} = 0.0279 \cdot (PW_e \cdot 10^{-3}) + 0.6816; \quad for\ (PW_e \cdot 10^{-3}) \leq 200kW \tag{13}$$

The listed actual systems can handle input power up to 200kW we therefore limit the specific power to this maximum value our multi-megawatt system. It is envisioned multiple converter units are used. We assume these units are designed to high efficiency standards and use a value of 98% [54][55][56][57]. If we assume the spacecraft generates 50 MW for the NEP system approximately 1 MW must be dissipated by Radiator 2 for the PMAD system. We assume that the maximum operating temperature of the system is 250 ^oC (523 K). This configuration is designed to operate at 200 ^oC (473 K) using SiC power converters. This results in approximately 900 m^2 in radiator area when converting 48.5 MW coming from the alternator. Together with the Alternator, this results in 2500 m^2 in radiator area. A value close to the entire radiator size of the NASA NEP-CP 1.2 spacecraft.

11. Power Distribution Cable

The power distribution cable is the main cable to send electricity from the power converter in the PMAD to the electric thrusters. We separated this part from the PMAD system due to modeling for the correct voltage based on the electric propulsion thruster used, sizing the wire for self-cooling, and ensuring the transmission efficiency was over 99.2%. For our concept we assumed 200 meters of cabling would be required. This length is based on the estimated size of the radiator. A relationship for the mass of the cable was found given the line voltage and transmission power.

$$m_{cable} = 2.349 \cdot 10^{10} \cdot V_{cable}^{-1.984} \cdot (PW_{cable} \cdot 10^{-6}) \tag{14}$$

12. Electric Propulsion Thrusters

Nuclear electric propulsion (NEP) is a critical subsystem for this mission. A high specific impulse NEP system arranged along with a high thrust delivering NTP system allows for a fuel efficient, faster transit time to be feasible. As such, the NEP subsystem needs to be selected such that one gets the most optimal system performance for a given mission. In regards to Fast-Transit missions to Mars, the most important parameter is to effectively package the electric thruster into a low mass to power ratio. Other parameters to consider in system integration and selection are heat and power, size duty cycle, stability, propellant storage, firing time, life time, and complexity. Additionally, the ability of the thruster to produce the required thrust becomes an important factor. For electric propulsion thrusters, the I_{sp} is related to the thrust by,

$$\frac{T}{PW_e} = \frac{2\,\eta_{et}}{I_{sp}\,g} \tag{15}$$

We see that a high I_{sp} thruster may not provide the required thrust to quickly transit between two planets. Fig. 10 shows the notional operating range of different thruster technologies. The figure has a red line to denote the designed for NTP I_{sp} of the WREN system (Table 1). Any electric thruster technology to the left of the line could be replaced by the WREN NTP system. The most important parameter becomes the thruster efficiency that can be designed to for each thruster. We see that magnetoplasmadynamic (MPD) thrusters have the ability to provide a high thrust to power ratio. The thrusters can be configured as Self-Field (SF) or Applied Field (AF). SF-MPD technology can generally provide a better thrust per power performance. We see that the SF-MPD is in a similar I_{sp} regime as the WREN NTP system in Fig. 10. Therefore, AF-MPD was explored for this work. With the state-of-the-art thrusters such as MPD thrusters, having a high input power results in high current density causing the cathode meltdown, thus bringing the thruster to the end of its lifetime at an alarming rate [58]. We therefore need to model both the thruster and the required thruster subsystems to keep the thrusters cool. This is true for all thruster technologies, Fig. 10 shows the efficiency of such systems range from 30 to 70 % efficient. Another issue is that most state-of-the-art thruster technology is only scaled to 100s of kW due to limitations of current NEP electrical power generation systems. Specifically, having a high input power results in high current density causing the cathode meltdown due to thermodynamic constraints in dimentional scaling. This results in a "scaled up" thruster having a significantly shorter lifetime [58]. We therefore have to rely on already conducted scaling studies to predict the performance of parameters of the MPD thrusters instead of simple extrapolation. A recent review on key performance parameters for Mega-Watt NEP elements [42] listed a power per thruster target and a threshold value of 1.0 and 0.5 MW_{et} respectively. Additionally, NASA Glenn's VF-1 vacuum chamber can test up to 1 MW MPD thrusters [59]. We therefore limit our per thuster to a 1 to 1.5 MW_{et} value out of practicality. Although Mega-Watt thrusters have been demonstrated, the majority of tests have been relatively short compared to transit times to Mars [60]. Significant research is required to enable use for the high-power requirements for a Mars Fast-Transit as discussed in later sections of this paper. Work by Gilland [61] conducted modeling work for MPD thrusters ranging in I_{sp} from 2,000 to 10,000 seconds. The paper is unique in that the thruster sub-components such as the PMAD and electrical cabling are removed from the power to mass ratio calculation and supplied a value just for the MPD thuster and the required radiator for cooling. The study evaluated thusters designed for 1, 2.5 and 5 MW_{et}. For a power of 1 MW_{et} and an I_{sp} of 3000 sec, α is listed as 0.5 kg/kW_e. The motive gas studied was hydrogen, but we will assume the scaling parameter closely approximates other fuel types. A recent review paper [62] on nuclear space propulsion, Table 3.3 lists a lithium MPD thuster having an α of 0.5 kg/kW_e with a power rating of 245 kW. We therefor use this value of α for our analysis.

As explained in following sections, our current strategy is limited to a constant acceleration burn for the NEP system with a resulting constant I_{sp}. Other systems such as VASIMR [63] found that a variable I_{sp} provided mass savings over the trajectory burn. We plan to alternatively look at a mix of high and low power thrusters to provide variation in the thrust profile of the NEP burns as our trajectory modeling capabilities are improved.

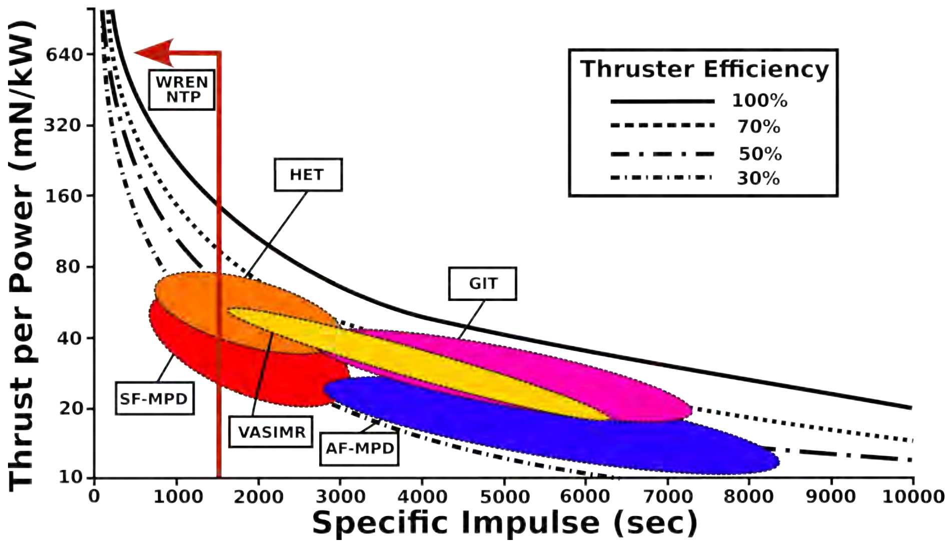

Fig. 10 Approximate relationship between I_{sp} and specific thrust for a range of electric thruster technologies. Adpated from [64].

Table 1 Initial Mars mission WREN cycle performance metrics.

NTP Mode	
Exhaust Temperature(K)	4765
Exhaust Velocity (km/s)	14019
Isp (sec)	1430
Thrust (kN)	34.7
Thruster Power (MW)	228
Specific Mass (kg/kWth)	0.44
Thrust/Weight	0.035

NEP Mode	
Electric Power (MW)	48.28
Thruster Efficiency (%)	50
Isp (sec)	3000
Thrust (kN)	1.57
Thruster Power (MW)	24.14
Specific Mass (kg/kWe)	2.09
Thrust/Weight	0.002

B. Performance of Initial Bi-modal Concept Design

As an initial design of the propulsion system, we assumed that the I_{sp} of the NTP should be maximized while being within materially manageable, dissociated hydrogen exhaust temperatures. We also specified an NTP thrust of 34.7 kN as this was on the low end of past NTP rocket designs. The radiator acreage was constrained to 10,000 m^2 or less. As a

Table 2 Other important metrics of the initial WREN system. See Appendix for additional parameters.

	Mass (MT)
NTP Components	8.32
NEP Components	48.15
Shared Components	43.51
Total System	99.98

	Area (sq. m)	Mass (MT)
Radiator 1	38.97	0.117
Radiator 2.1	5555	16.67
Radiator 2.2	4400	13.20
Total	9994	29.98

Core Power (MW)	NTP Mode	NEP Mode
NTP Reactor Core	94.66	Shut Down
Brayton Reactor Core	337.2	189.5

	Mode	Mass Flow Rate (kg/s)
Motive Gas	NTP	2.475
Driver Gas	NTP/NEP	10.15

comparison, the NASA NEP-CP Vehicle 1.2 was designed with a radiator on the order of 2,500 m^2. We assume that a larger radiator, by a factor of 4, could be justified if the transit time and other system masses could be significantly reduced. The compression ratio of the NTP Wave Rotor was set to enable an I_{sp} of 1430 sec for the NTP mode as shown in Fig. 1. The NEP alternator is not engaged ensuring that the power generated by the Brayton cycle goes into the NTP wave rotor for heating the motive gas. During NEP mode, Compressor 2 is disengaged from the turboset and the Brayton cycle gas by passes the NTP wave rotor. It was found that 48.28 MW of electricity is available at the end of the power distribution cable for the NEP thrusters. The total propulsion mass was almost 100 MT (metric tons) (Table 2). This led to a mass to power ratio of 2.09 kg/kW_e for the NEP propulsion mode. The NEP components make up the greatest contribution to mass as shown in Fig. 11. In the figure, "Other" refers to the LH_2 Turbopump, LH_2 Recuperator, and the mass of both wave rotors. If significant mass savings are sought, improvements to the electric thruster power density are most significant after the radiators. For completeness, a full list of pressures and temperatures of the NTP motive and Brayton cycle gas (both NTP and NEP mode) are listed in the Appendix.

Finally we must note that the radiators operate at high inlet temperatures. A large amount of nuclear reactor energy is then wasted. We plan to explore the use of thermoradiative thermal energy conversion devices for production of additional electrical energy that could be used to recover waste heat from the Brayton cycle [65][66]. The temperature of Radiator 1 is also high enough that high temperature solar cells may be able to be effectively employed to recover the waste heat. We plan to add these subsystems to our modeling as the Matlab OOP program is matured.

C. Comparison to Other Rocket System Technologies

Fig. 12 shows the performance of many different flown and studied in-space nuclear electric power systems. The x-axis lists the total system electric power provided and the y-axis lists the specific power of the energy generation/propulsion system. We see that the inclusion of a wave rotor to the Brayton allows for the WREN NEP performance to pass what was believed to be the NEP Turbo-Generator Limit. This is mainly due to the ability of the Brayton Wave Rotor to process the gas from the nuclear reactor core at almost 2000 K (see Table 5 in the Appendix). This high temperature along with significantly bringing up the Brayton cycle bottom temperature to 371 K and Radiator 2 inlet temperature of 790 K. This significantly reduces the area requirements of Radiator 2 compared to the colder radiator used for the NASA NEP/CP 1.2 design. Referring back to Fig. 12, only the notional Low-α Fusion concept provides both more total power and specific power capability for a NEP propulsion system.

Comparing both WREN NTP and NEP modes to other propulsion systems, Fig. 13 organizes them according to their vehicle acceleration vs. I_{sp}. Due to the ability of the Brayton cycle to provide a large electric power load to the electric thrusters, the system significantly falls out side of the vehicle acceleration of other Electro- systems. The WREN NTP conversely due to its increase in I_{sp} through a Brayton cycle process, has a significantly lower vehicle acceleration compared to other demonstrated thermal fission technologies. In Fig. 13 the power density is also mapped to the x-y coordinate systems. We see that the WREN NTP and NEP performance parameters line up with expected values between I_{sp}, vehicle acceleration, and power density. This gives confidence in the verification of the WREN propulsion modeling conducted for this work.

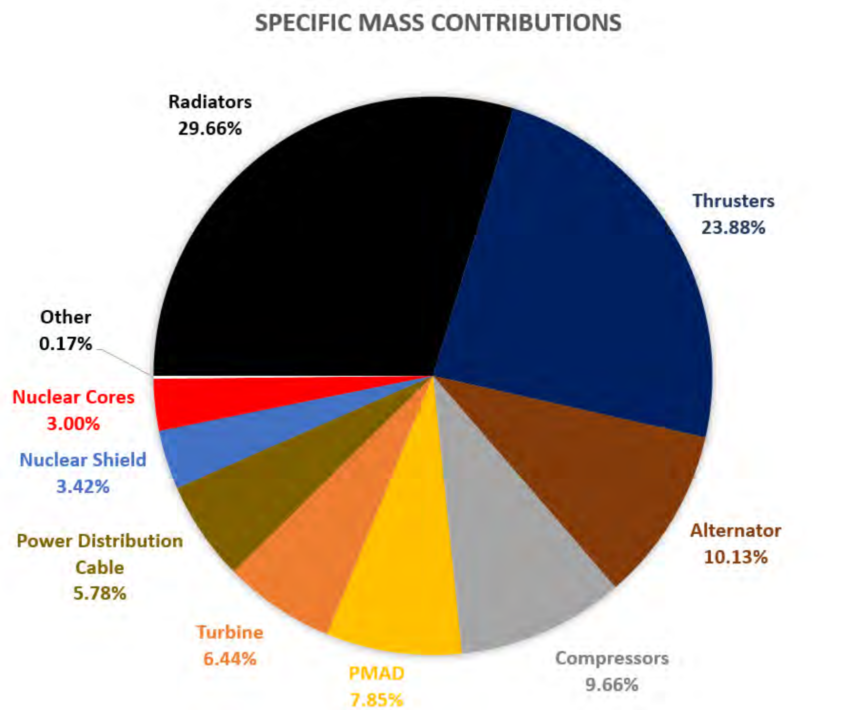

Fig. 11 Specific Mass Contributions of the WREN System sub-components.

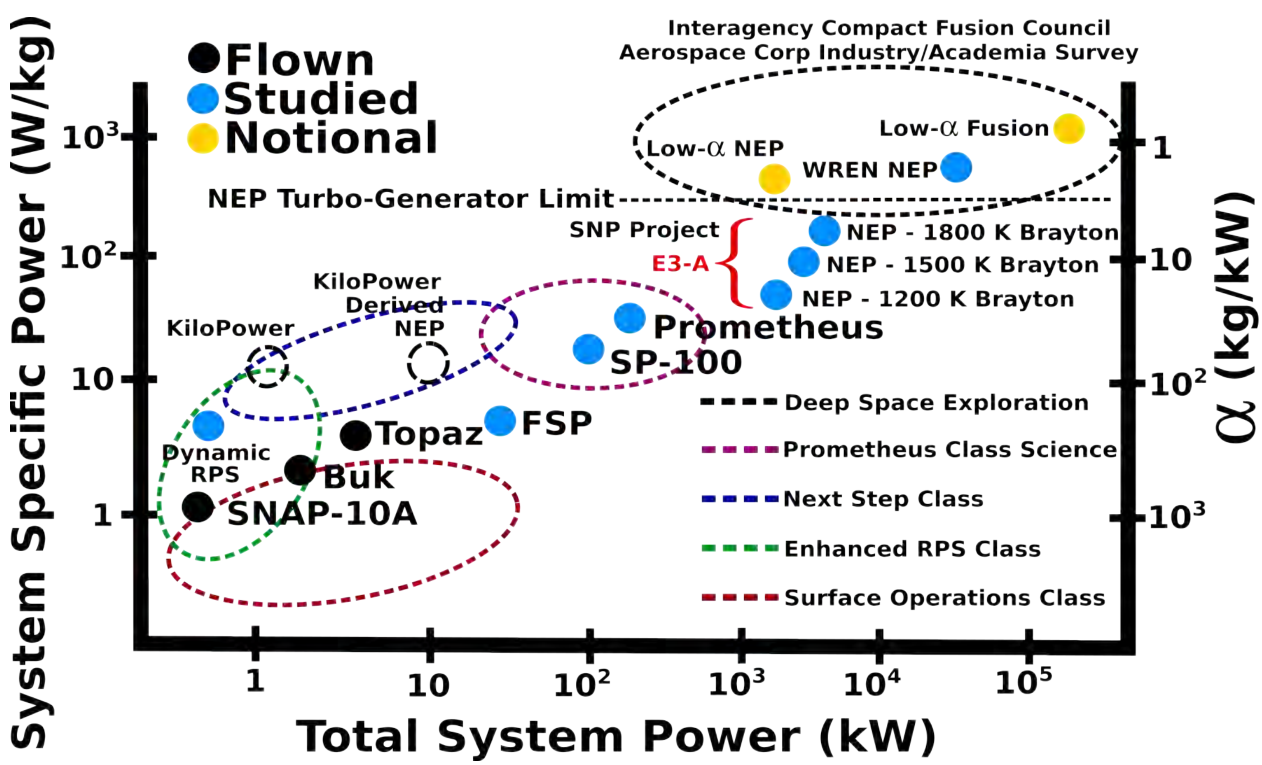

Fig. 12 Comparison of WEN NEP mode to other NEP system classes.

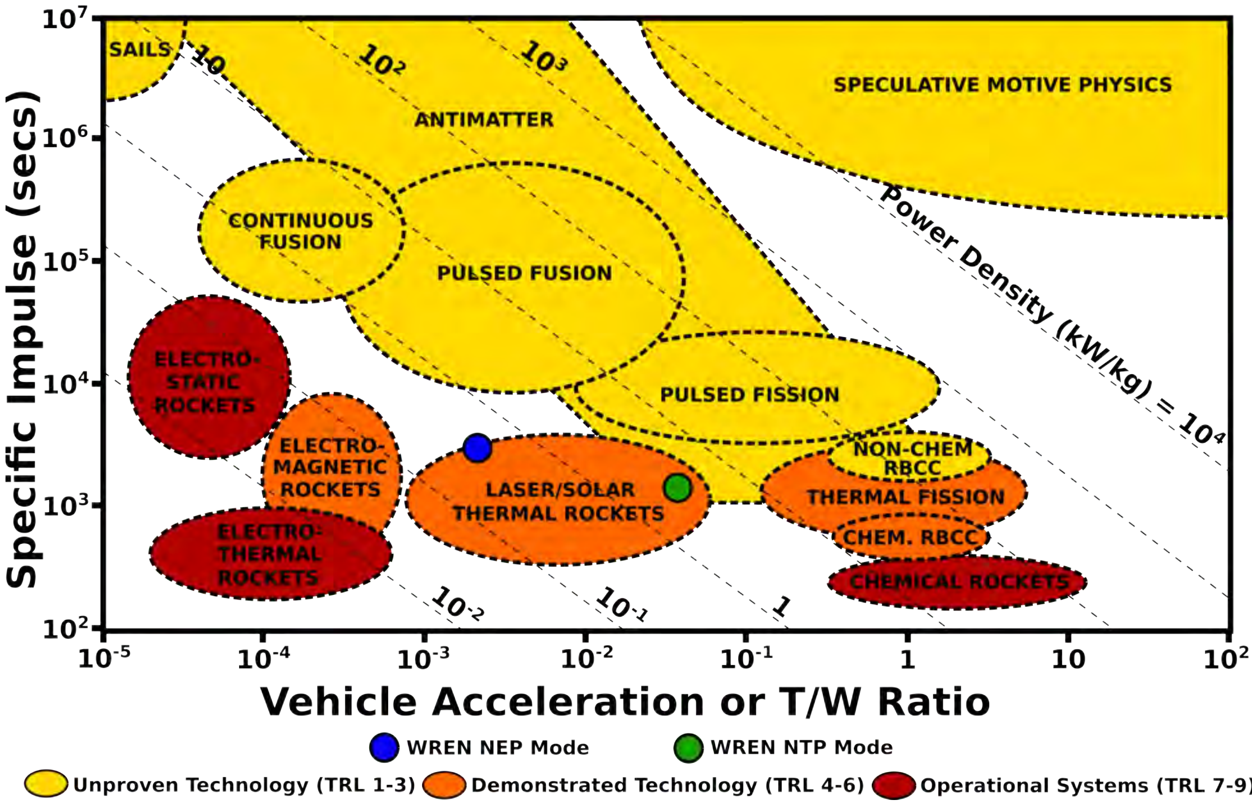

Fig. 13 Comparison of WEN NEP mode to other rocket propulsion technologies.

V. Human Mission to Mars Concept Vehicle

A. Spacecraft Overview

The inspiration for the development of this propulsion cycle was to significantly improve the NTP aspect of the bi-modal design. The NTP human mission to Mars report by Borowski[67] computed trajectories for a fast conjunction mission in the 2033 time frame. Table 3 lists the assumptions that they used for the NTP technology. Most impactful is the I_{sp} capability of 906-941 seconds. Compared to traditional chemical rocket propulsion (300-450 seconds) this is a substantial improvement. Their study proposed the NTP technology could reach Mars in a 150-220 day transit time. Additionally, the NASA Space Technology Research Grants Program issued a solicitation topic entitled "Revolutionary Propulsion for Rapid Deep Space Transit." One of the research objectives was developing propulsion systems enabling "Traversing the distance between Earth orbit and Mars orbit in no more than 45 days."[68] Our focus was to see how far we could improve this transit time with the WREN technology with the possibility of achieving the 45 days to Mars demonstration goal.

The WREN propulsion outlined in the previous section was further integrated into a Mars mission concept spacecraft. Fig.14 shows a rendering of the concept spacecraft orbiting Mars. Considerations such as placement of each sub-component, volume of fuel, and size of crew module were developed. Sub-component placements were dictated by the location of the Reactor Shield. Systems sensitive to radiation dosage, were placed in the cone shaped shadow of the reactor shield. This lead to the trapezoidal shape of the radiators and placement of the electric propulsion opposite of the rest of the propulsion system. In this analysis we considered a spacecraft using a current NASA crew habitat design. The habitat consisted of 45 MT of mass and can support a crew of 6 with supplies for 1000 days. The excess supplies are included as an emergency measure in case of propulsion system failure during transit to support potential rescue mission scenarios for the crew. The stored fuel is only for the Earth to Mars transit. A slower, more efficient cargo transport would bring the return fuel necessary for return to Earth. Since we are only concerned in the NASA demonstration of a 45 day transit, analysis of the requirements for the return to Earth leg was not conducted.

Table 3 2033 NTP human mission to Mars NTP system characteristics.

NTR System Characteristics		
Engine/Fuel Type		SNRE-derived / UC-ZrC "Composite"
Propellant		LH2
Thrust Level		25 klbf ("Pewee-class" baseline; 304 engine cluster on "Core" NTPS)
Fuel Element Length		1.32 m
Exhaust Temp		2790 - 2940 K
Chamber Pressure		~1000 psi
Nozzle Area Ratio		300:1
Isp Range		906 s (2790 K) - 941 (2940 K)

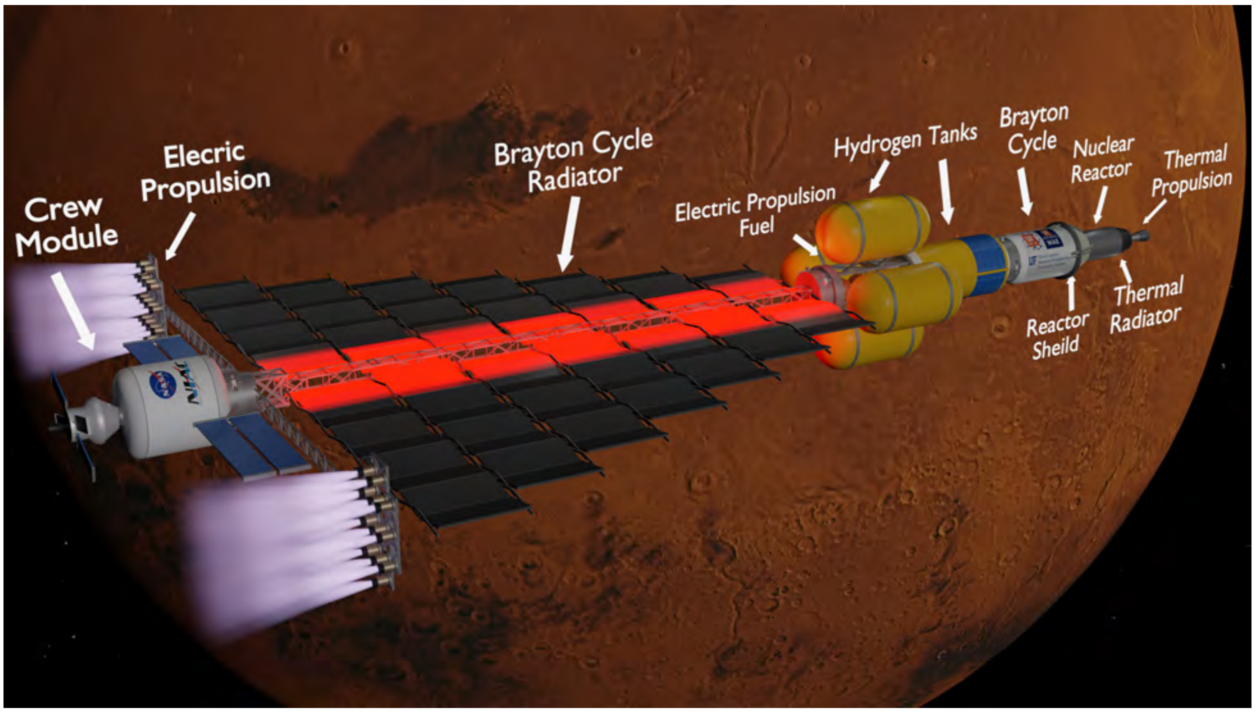

Fig. 14 WREN human Mars mission concept spacecraft.

B. Fast-Conjunction Class Mars Missions

In this section we focus on the transfer to Mars. For low I_{sp} propulsion systems like chemical propulsion, missions are constrained to using a Hohmann transfer orbit that typically gives the lowest ΔV. Ocassionaly the planets are aligned such that a fly-by of Venus can reduce this expense even further. Fig.15 shows such a case. These types of maneuvers are considered Opposition class missions. These mission unfortunately consist of long transit times (200 - 400 days). Shorter transit times can be made using larger impulsive burns. This class is referred to as Fast-Conjunction missions. Here the spacecraft leaves when the Earth starts to overcome Mars. The timing sets the offset between the planets as shown in Fig.15.

For the Mars mission, the NTP mode is used to quickly deorbit/orbit a planet due to its relatively large thrust compared to the NEP systems (Table 1). The maneuver is typically assumed to be impulsive in nature and can be approximated by the Tsiolkovsky rocket equation.

$$\Delta V = v_{exit}\, ln \frac{m_i}{m_f} = I_{sp} g\, ln \frac{m_i}{m_f} \tag{16}$$

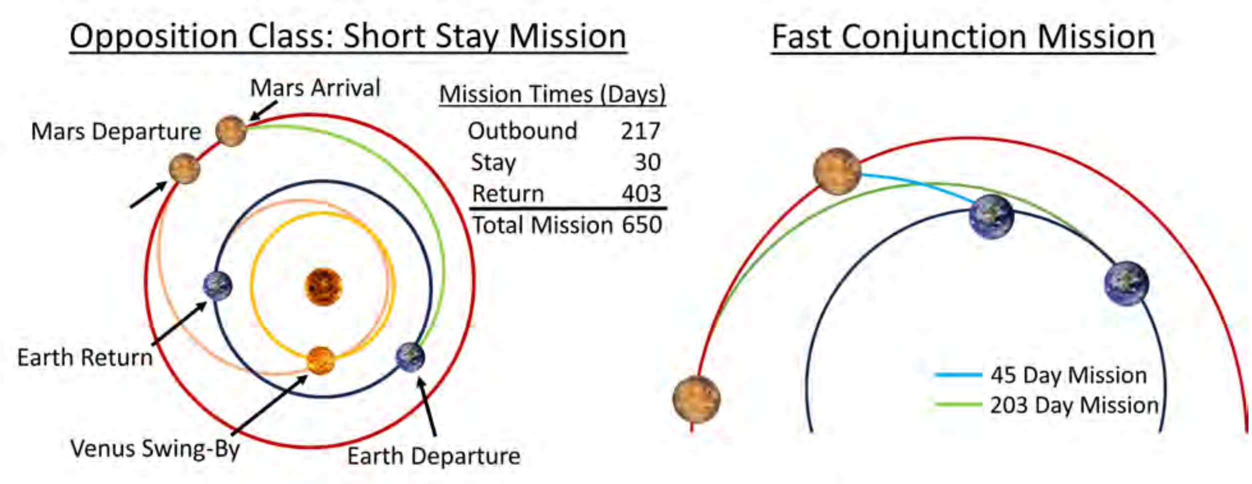

Fig. 15 Opposition and Fast-Conjunction Class Mission Trajectories.

The NTP Human Mission to Mars report by Borowski[67] computed trajectories for a fast conjunction mission in the 2033 time frame. They explored transit times ranging from 60-220 days for the outbound Earth to Mars leg. We used the ΔV values from these results to extrapolate the required values for a 45 day mission. For Earth departure a ΔV of 10.4 km/s was estimated to be required and for Mars arrival the value was 11.4 km/s. Comparatively, a 220 day mission only required 3.6 km/s for Earth departure and 1.3 km/s for Mars arrival. Referring to equation 16, if we want to have the same initial spacecraft mass as a chemical rocket (I_{sp} = 450 sec) the advanced propulsion system would require an I_{sp} of 2000 sec for the 45 day transit. If we want to have the same initial mass as current NTP technology (I_{sp} = 900 sec) the advanced propulsion system would require an I_{sp} of 4000 sec. The NTP mode of the current WREN design is only 1430 sec. Therefore an NTP only WREN system would not provide a practical initial spacecraft mass for the 45 day mission.

We now consider an NEP only system for the Earth to Mars leg. It would require the space vehicle to conduct a spiraling orbital transfer maneuver, which can take many days to complete. As an example, the Variable Specific Impulse Magnetoplasma Rocket (VASIMR) technology is a multi-metawatt advanced nuclear reactor power source. A study was conducted to analyse if the technology would be able to travel to Mars in 39 days.[63] Their concept spacecraft required an approximately 200 MW NEP propulsion system to quickly leave Earth's orbit. Their mission relied on a direct entry of the Mars landing craft that would slow down using an aerobreaking maneuver. The main spacecraft conducted an orbiting maneuver lasting 30 days. The crew module ranged in size from 20 to 30 MT to support a crew of 4 astronauts. Their concept indicted that the NEP system would require a α_{NEP} of 0.5 to 1.0 kg/kW$_e$ depending on the departure orbit from Earth. Referring to the performance specifications of the current WREN configuration, the NEP mode alone can not practically close a mission similar to VASMIR.

In order to approximate fuel requirements, a systems level trajectory model was developed to handle the bi-modal nature of the WREN propulsion system. Due to the low thrust of the NEP subsystem, this analysis requires the inclusion of the acceleration capability of the space vehicle during the use of the NEP subsystem. This parameter can be derived by inference of α_{NEP}, shown in Eq. 17.

$$\alpha_{\mathrm{NEP}} = \frac{2\eta_{et}}{\lambda}\left(\sqrt{1+k} - \sqrt{k + \frac{m_{\mathrm{PL,NEP}}}{m_i}}\right)^2 \tag{17}$$

where η_{et} is the efficiency associated with power conversion of the NEP thrusters, λ is the trajectory characteristic parameter, k is the structural coefficient of the space vehicle, and $m_{\mathrm{PL,NEP}}$ and m_i are the masses associated with the payload carried by the NEP system and initial state of the vehicle at the start of the operation of the NEP system, respectively. The structural coefficient is defined by

$$k = \frac{m_{\mathrm{S}}}{m_{\mathrm{p}}} \tag{18}$$

where m_{S} is defined as the tanks structure mass and m_{p} is the propellant mass.

The mass budget of the spacecraft is defined as a cumulative total of all of the subsystem masses, represented in Eq. 19.

$$m_{\text{i,tot}} = m_{\text{PL}} + m_{\text{p}} + m_{\text{S}} + m_{\text{PP}} \tag{19}$$

For the bi-modal concept, special care must be taken in assigning the proper system masses. In efforts not to modify the governing equation, Eq. 17, the propellant mass is accounted as three separate values.

$$m_p = m_{\text{p,Ed}} + m_{\text{p,Ht}} + m_{\text{p,Ma}} \tag{20}$$

where $m_{\text{p,Ed}}$ is the propellant used during Earth departure, $m_{\text{p,Ht}}$ is the propellant used during Heilocentric transit, and $m_{\text{p,Ma}}$ is the propellant used during Mars arrival. When applying Eq. 17, $m_{\text{p,Ma}}$ is included as part of $m_{\text{PL,NEP}}$. We also need to add the mass of propellant tanks for the Earth departure burn to m_i is they are not ejected as part of a staging strategy. We use the same value for the tank structural coefficient for both NTP and NEP motive gas tanks. The propulsion system mass contains all the components to enable operation of both modes. Traditionally α_{NEP} is defined as

$$\alpha_{\text{NEP}} = \frac{m_{\text{PP}}}{P_e} \tag{21}$$

where it is assumed that m_{PP} completely scales with the electric power required for the NEP mode. In our case,

$$m_{\text{PP}} = m_{\text{PP,NTP}} + m_{\text{PP,NEP}} + m_{\text{PP,shared}} \tag{22}$$

we have sub-components that are exclusive to the NTP mode ($m_{\text{PP,NTP}}$) and the NEP mode ($m_{\text{PP,NEP}}$). There are also sub-components that are shared between the modes ($m_{\text{PP,shared}}$). For instance, the Brayton cycle components are used by both modes. From a fundamental perspective it is unclear how α_{NEP} defined in Eq. 17 should be treated. For instance, the NTP mode may require an excessively large power from the Brayton cycle compared to the NEP model or vice versa. In our analysis we ignored this issue and assume that the Brayton cycle would be fully utilized by the NEP system providing theoretically maximum electric power for the NEP mode. Referring to Fig. 11 we see that subsystems used only by the NEP make up a significant mass of the propulsion system. If the power required by the NEP to satisfy the trajectory requirements is in reality lower, the assumptions in Eq. 17 may be too conservative in regards to the ratio of payload mass to initial mass. This completes making Eq. 17 consistent for use in a bi-modal propulsion system for the Fast-Conjunction mission. The final mass of the spacecraft is found by

$$m_f = m_{\text{i,tot}} - m_{\text{p}} - m_{\text{S,staged}} \tag{23}$$

where $m_{\text{S,staged}}$ is the mass of any tanks ejected after a propulsive burn. We ignored this parameter in this work.

In Eq.17, the trajectory characteristic parameter is a non-trivial parameter to compute. It represents the integral of the acceleration squared over the spacecrafts trajectory, given in Eq. 24.

$$\lambda = \int \gamma_{\text{acc}}^2 dt \tag{24}$$

An ideal estimate of the ΔV required by the NEP mode is found by integrating the acceleration profile and draws analogy to the classic rocket equation.

$$\Delta V_{\text{ideal}} = \int \gamma_{\text{acc}}\, dt = v_{exit} \cdot \ln\left(\frac{m_f}{m_i}\right) \tag{25}$$

We can also link the mass flow rate of the NEP motive gas ($\dot{m}_{et}$) and I_{sp} to the required electrical power from the Brayton cycle alternator (PW_{e}) using:

$$\frac{1}{2}\dot{m}_{et} \cdot \left(g \cdot I_{\text{sp,NEP}}\right)^2 = \eta_{\text{et}} \cdot PW_{\text{e}} \tag{26}$$

Where η_{et} is the efficiency of the electric thrusters and g is the Earth gravity acceleration at sea-level. A variant of the rocket propulsion equation can be formed for power-limited systems.[69]

$$\int_{t_o}^{t_f} \gamma_{\text{acc}}^2 dt = 2\eta_{\text{et}} \cdot PW_e \cdot \left(\frac{1}{m_f} - \frac{1}{m_i}\right) \tag{27}$$

Using optimization methods,[70] the payload mass fraction can be found using the expression:

$$\frac{m_{\mathrm{PL}}}{m_i} = 1 - \frac{k+1}{1 + \left(\frac{2\eta}{\lambda}\right)\left(\frac{PW_e}{m_i}\right)} - \alpha_{\mathrm{NEP}} \cdot \left(\frac{PW_e}{m_i}\right) \tag{28}$$

If we assume that the payload to initial mass ratio is independent of the other variables, Eq. 28 is used to produce Eq. 17.

The VASIMR study conducted full trajectory analysis varying the transit time to more exactly compute the ΔV and initial mass requirements for their concept spacecraft. It was found that the trajectory characteristic for their mission was able to be represented as a simple function with only minor uncertainty by,

$$\lambda(t_{trans}) \approx a \cdot t_{trans}^{b} \tag{29}$$

where a = $5.22 * 10^7$ and b = -2.9183 are coefficients fit to their trajectories and t_{trans} is the transit time measured in days. This allowed for further studies on the VASIMR system using a similar system of equations presented in this section for their NEP burns. We used these values to verify the results of our system of equations with only using the NEP mode of the WREN cycle. For analysing the bi-modal system, we can't use the VASMIR data due to the spiral maneuver conducted by the NEP thrusters at Earth departure. As the desired transit time is shortened from hundreds of days to 39 day, the spiral maneuver significantly contributes to the required trajectory characteristic. We plan to use the NTP mode to quickly leave the Earth-Moon system using an impulsive burn. We therefore just require a representative acceleration profile during the heliocentric phase of the mission trajectory. If we assume that the NEP mode is employed using constant acceleration over the trajectory, Eq. 24 becomes a simple linear equation. We also note that for the Fast-Conjunction mission, Earth and Mars are always fixed distances over a given transit period. Therefore heliocentric phase of Eq. 29 may be correlated through the distance formula.

$$x = v_i \cdot t + \gamma_{acc} t^2 \tag{30}$$

If we include v_i we are able to compute the required acceleration for the heliocentric phase. These assumptions will not led to optimum performance values, but are suitable for understanding the performance of our system without conducting full trajectory calculations. Solving for the trajectory characteristic,

$$\lambda = (x - v_i \cdot t)^2 \cdot t^{-3} \tag{31}$$

The form is relatively close to the VASMIR correlation form. Referring now to the work of Borowski [67] that studies a pure NTP propulsion system, the acceleration is zero giving us a way to solve for x providing a leading coefficient that can be corrected with different initial velocities. It must be noted again this is not finding the correct distance traveled, but a distance that correlates to a required λ given an initial departure velocity. We found that this approximation gives consistent results for transit times less than 65 days. For longer travel times losses due to gravity and the thrust vector become too large. This can be visually seen by the trajectories computed by Dankanich [71] for the VASIMR design. Additionally, the VASIMR work showed that for mission Earth to Mars legs with transit times in excess of 100 days, the NEP spiral orbits become less challenging suggesting a pure Multi-Megawatt NEP system may provide a theoretically simpler solution than a bi-modal NTP/NEP design. In our next steps we plan to conduct full trajectory calculations for the Earth to Mars leg using the Copernicus software[72]. Results will be compared to this simplified model to understand the uncertainty in our assumptions.

C. Earth to Mars Mission Leg

In our work we are not currently focusing on an entire Mars mission, but just the Earth to Mars mission leg to demonstrate the technology capability. This is a similar practice used when initially studying the VASIMR technology. This isolates propulsion system performance metrics removing impacts such as Mars stay times and return leg strategies that complicate the analysis. We consider transporting a crew of 6 with enough supplies for 1000 days. The excess supplies are included as an emergency measure in case of propulsion system failure during transit to support potential abort and rescue scenarios. This habitat is similar to the one being used for NASA baseline mission studies[1]. Fig. 16 shows the concept of operations of the spacecraft. The spacecraft departs Earth from a Near-Rectilinear Halo Orbit (NRHO) after assembly as shown in Fig. 17. As the spacecraft passes Earth, a NTP mode burn is conducted. After the burn maneuver, the NTP mode is turned off and a slow-spin maneuver is conducted over a period of a few hours. Small reaction control jets are used for this low ΔV spin maneuver and considered part of the structural mass. During the

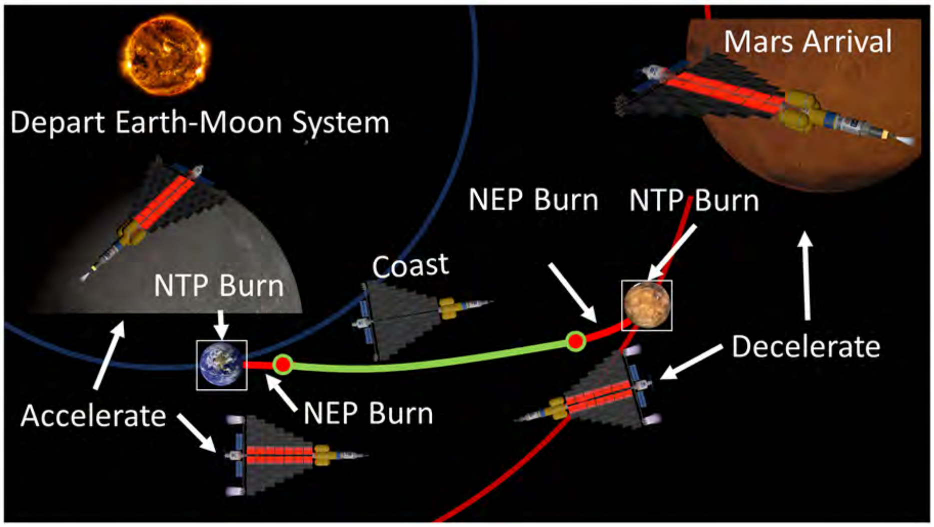

Fig. 16 Concept of operations Earth to Mars mission leg.

maneuver NTP components are cooled and the nuclear reactor is moderated in preparation for the NEP mode. Once the electric thrusters are positioned correctly, the NEP burn starts. Fig. 16 shows a coast period where the NEP mode is turned off. In this work we consider a constant thrust strategy resulting in no coasting period. We include this state of the spacecraft since work on other NEP propulsion systems find a coasting period results in a minimized initial departure mass. Next the spacecraft positions the electric thrusters to start a NEP burn to slow the spacecraft down as it approaches Mars. It then performs another spin maneuver in order to ready the spacecraft for the final NTP burn to orbit Mars. In comparison, the VASMIR mission assumed the crewed landing module would conduct a direct entry into Mars atmosphere while the spacecraft would slow down over a multi-day period to park in Mars' orbit.

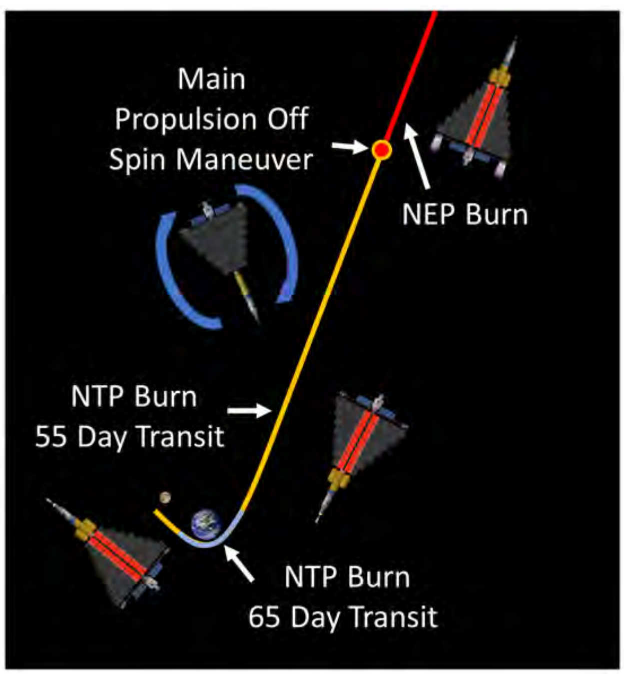

Fig. 17 Concept of operations for departure from Earth-Moon system.

Table 4 shows estimates for a notional 45 day transit using the equations outlined in this work. The initial mass of the spacecraft was found to be 530 MT. This is heavier than the NASA NEP-CP Vehicle 1.2 (382 MT). Though the NEP-CP system has a transit time of approximately 382 days. To obtain similar masses, the crewed module would need to be reduced to 4 with a resulting redesigned module to realize mass savings. A pure NTP spacecraft studied by NASA had an initial mass of over 600 MT resulting in a 297 day transit. Exact comparison is hard to make due to the two NASA reference mission spacecraft are designed for a full mission scenario. The main take away is the 45 day transit using WREN propulsion produces a spacecraft in the range of initial mass similar to NASA baseline designs.

Table 4 Summary of spacecraft masses and ΔV burns for 45 Day Earth to Mars leg.

Bi-Modal Trajectory Estimate from Power Limited Propulsion Equation						
Transit Time	**45**					
Crew Vehicle (MT)	**45**	**Propulsion (MT)**	**100**	**Payload (MT)**	**145**	
Traj. Stage	**Cycle**	**Initial Mass (MT)**	**Final Mass (MT)**	**Fuel Mass (MT)**	**Fuel Tank Mass (MT)**	**ΔV (km/s)**
ED Burn	**NTP**	**530**	**396**	**134**	**15**	**4.1**
Transit Burns	**NEP**	**381**	**257**	**124**	**14**	**14.5**
MA Burn	**NTP**	**253**	**156**	**97**	**11**	**6.8**

The main motivation for a fast-transit trajectory is to reduce the risk of human crew. Learning from experiences of astronauts living on the International Space Station (ISS), many health risks arise due to zero-gravity. Additionally, radiation from the Sun and cosmic space significantly contribute to the total radiation exposure of the crew over a mission. Reducing the transit to 45 days significantly reduces these risks compared to the traditional long duration transits, but how much risk is removed between a 45 day vs. 65 day transit? Fig. 18 shows estimates of initial departure mass vs. transit time. By making the trip just 5 days longer, significant initial mass savings can be achieved. For a 65 day transit the initial mass is almost half. The figure also shows the impact of different NTP mode ΔV burns for Earth departure. To remove our concerns with the rough estimation of the NEP trajectory characteristic, we see that trading NTP vs. NEP burn time is relatively insensitive due to the high I_{sp} if the NTP mode. It should be noted again that if we use a pure NTP burn as in Borowski [67] it is clearly impractical.

Finally a main weakness of the presented performance of the WREN system is the low thrust to weight ratio of the NTP mode. For the initial spacecraft masses and ΔV required for NTP burns, the burn can not be assumed to be instantaneous. Referring to other NTP spacecraft [67] the burn times should be on the order of 30 minutes to 2 hours for impulsive maneuvers. This analysis shows the WREN NTP burn times are on the order of 8 to 15 hours in duration. This has a large impact on the requirements of nuclear core technology where NERVA class systems have never been tested for such duration. Future trajectory analysis will require finite burn modeling of the NTP modes to understand the impact of gravity losses. Fig. 17 presents a notional description of the difference in burn time with respect to the trajectory for a 55 and 65 day Earth departure NTP burn. In a worst case scenario, Earth departure and Mars arrival would have to be conducted using a spiral maneuver. For the 39 day VASIMR mission, it required on the order of 200 MW electric power to quickly leave Earth's orbit for their 39 day Earth to Mars leg. The WREN NTP mode has a thrust power of approximately 200 MW equating to approximately 400 MW electric power if VASIMR is operating at 50% thruster efficiency. Unfortunately the trajectory characteristic reported in the VASIMR studies lumps in the contribution of Earth departure, Heliocentric transfer, and Mars arrival burns. Making it impossible to be used for a bi-modal system trajectory analysis. We therefore plan to look into detailed trajectory modeling to better understand this issue.

Ultimately, these results may be indicating that the NTP I_{sp} and the NEP thrust power are too large for this mission. In regards to NTP burns, a similar phenomena was found with the LO_2-Augmented Nuclear Thermal Rocket (LANTR)[73]. In this concept additional LO_2 was added in an after-burner to enhance the thrust performance of the NTP rocket for operation in the Earth-Moon system. In the case of the WREN system, the compression ratio of the NTP Wave Rotor can be designed to mission requirements trading I_{sp} for thrust. Referring to Fig. 11 the NEP only subsystem components make up a significant contribution to the propulsion mass. Full trajectory analysis is needed to explore if such a high NEP thruster power is required. Fig. 18 shows that trading between Earth departure ΔV (NTP) and required NEP acceleration provide similar results as we reach a 45 day transit time. Removing NEP propulsion mass will help with the NTP Earth departure burn and may off set the losses of less power available during the heliocentric phase. Again detailed trajectory modeling is required to better understand these issues.

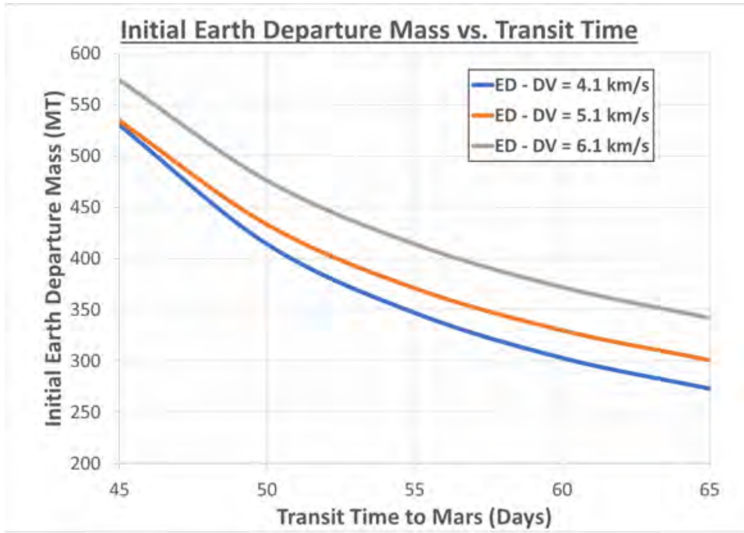

Fig. 18 Initial Earth Departure (ED) Mass vs. Transit time for different Earth departure burns of the NTP mode.

VI. Conclusion

A systems level model of a bi-modal NTP/NEP propulsion system was developed. Through the use of wave rotor technology, both NTP and NEP propulsion parameters were significantly improved. A simplified trajectory analysis model was developed to explore the capability of an non-optimized configuration. It was found that the system provided significant improvement in its ability to conduct a Fast-Transit mission to Mars. Though the system results in reasonable initial masses for a concept spacecraft traveling to Mars in 45 days, significant mass saving can be realized by increasing the transit time by just 5 to 20 days. It is suggested that a full mission profile should be explored to understand the implications of having to minimize transit time for both the outbound and return leg of a human Mars mission. Either way, this propulsion system technology demonstrates the ability to easily conduct Fast-Transit missions to Mars.

Acknowledgments

Portions of the work were funded by the NASA NIAC program through grant number 80NSSC23K0589. We would like to acknowledge Prof. William Lear, Dr. Gerard Welch, Dr. Dan Paxson, and Dr. Robert Kielb for their discussions on wave rotor technology. To Dr. Kurt Polzin for his discussions on nuclear reactor and electric propulsion technology development. To Prof. Christopher Petersen for his discussions on mission trajectory optimization. Also, the NASA NIAC program personnel (Michael LaPointe, John Nelson, Ron Turner, Kathy Reilly, Frank Spellman, Mau Nguyen, and Micah Bullard) and external council (Mae Jemison, David Brin, Louis Friedman, Amy Kronenberg, Edgar Zapata, and Merri Sanchez) for their discussions on the technology during the NASA NIAC Phase I activities.

Appendix

The pressure and temperatures of the two propulsion gas loops are listed here in the Appendix in Table 5 for completeness. Station positions are labeled in Fig. 9. As detailed in the figure, underlined values specify the port conditions surrounding the NTP Wave Rotor during the NTP mode which results in the optimized I_{sp} of the thermal rocket. Values highlighted in red and blue represent the port conditions surrounding the Brayton Wave Rotor for the NTP and NEP mode, respectively. Note that these value counterparts between modes surrounding the Brayton Wave Rotor are equivalent (e.g. $p_{1Be} = p_{1Bt}$), indicating the OOP model successfully balanced the modes. Pressure values were set based on requirements for the NTP rocket nozzle and nuclear reactor cores.

Table 5 Pressure and temperature values at their respective stations based on Fig. 9.

Station Pressures (kPa)		Station Temperatures (K)	
NTP Mode Motive Gas Cycle			
p0	139.27	T0	20.39
p1	701.09	T1	21.00
p2	687.34	T2	507.35
p3	673.86	T3	2850.00
p4	2540.46	T4	4764.99
NTP Mode Driver Gas Brayton Cycle			
p0Bt	88.49	T0Bt	369.12
p1Bt	179.64	T1Bt	466.17
p2Bt	858.67	T2Bt	790.14
p3Bt	841.84	T3Bt	507.35
p4Bt	4217.70	T4Bt	850.53
p5Bt	4135.00	T5Bt	2850.00
p6Bt	859.36	T6Bt	2151.75
p7Bt	842.17	T7Bt	1973.97
p8Bt	340.02	T8Bt	1650.00
p9Bt	92.07	T9Bt	1246.62
p10Bt	90.26	T10Bt	507.35
NEP Mode Driver Gas Brayton Cycle			
p0Be	90.26	T0Be	371.84
p1Be	179.64	T1Be	466.17
p2Be	858.67	T2Be	790.14
p7Be	842.17	T7Be	1973.97
p8Be	340.02	T8Be	1650.00
p9Be	92.07	T9Be	1246.62

References

[1] Oleson, S. R., Burke, L. M., Mason, L. S., Turnbull, E. R., McCarty, S., Colozza, A. J., Fittje, J. E., Yim, J. T., Smith, M., Packard, T. W., et al., "Compass Final Report: Nuclear Electric Propulsion (NEP)-Chemical Vehicle 1.2," Tech. rep., 2021.

[2] Robbins, W., "An historical perspective of the NERVA nuclear rocket engine technology program," *Conference on Advanced SEI Technologies*, 1991, p. 3451.

[3] Nelson, S. T., Grey, J., and Williams, P. M., "Conceptual study of a liquid-core nuclear rocket," *Journal of Spacecraft and Rockets*, Vol. 2, No. 3, 1965, pp. 384–391.

[4] BARRETT JR, W. L., "Specific impulse of a liquid-core nuclear rocket," *AIAA Journal*, Vol. 1, No. 11, 1963, pp. 2649–2650.

[5] Allen, J., Johns, M., Patterson, M., Houts, M., Heidet, F., Smith, N. V., and Foster, J. E., "Overview of High-Performance Centrifugal Nuclear Thermal Rocket Propulsion System," *ANS Virtual Winter Meeting*, 2020.

[6] Houts, M. G., Thomas, L. D., and Nassersharif, B., "Centrifugal Nuclear Thermal Rocket Challenges and Potential," *45th Annual AAS Guidance, Navigation and Control Conference*, 2023.

[7] Thomas, L., Houts, M., Walters, W., Hollingsworth, K., Frederick, R. A., and Cassibry, J. T., "Establishing the Feasibility of the Centrifugal Nuclear Thermal Rocket," *AIAA Propulsion and Energy 2021 Forum*, 2021, p. 3604.

[8] Zhang, Y., "Advanced nuclear power engine: A brief overview of gas core reactor for space exploration," *International Journal of Advanced Nuclear Reactor Design and Technology*, 2023.

[9] Akbari, P., Nalim, R., and Mueller, N., "A review of wave rotor technology and its applications," *Journal of engineering for gas turbines and power*, Vol. 128, No. 4, 2006, pp. 717–735.

[10] Costiuc, I., and Chiru, A., "Evolution of the pressure wave supercharger concept," *IOP conference series: materials science and engineering*, Vol. 252, IOP Publishing, 2017, p. 012081.

[11] Welch, G. E., "Wave engine topping cycle assessment," *35th Aerospace Sciences Meeting and Exhibit*, 1997, p. 707.

[12] Nalim, M. R., Bane, S. P. M., Khan, M. J., and Jagannath, R., "Hybrid Wave Rotor Electric Aero Propulsion," *50th AIAA/ASME/SAE/ASEE Joint Propulsion Conference.*, 2014. URL `https://api.semanticscholar.org/CorpusID:209964013`.

[13] Weber, H., "Shock-Expansion Wave Engines—New Directions for Power Production," *Turbo Expo: Power for Land, Sea, and Air*, Vol. 79283, American Society of Mechanical Engineers, 1986, p. V001T01A025.

[14] Bellenoue, M., Boust, B., Vidal, P., Zitoun, R., Gaillard, T., Davidenko, D., Leyko, M., and Le Naour, B., "New combustion concepts to enhance the thermodynamic efficiency of propulsion engines," *Aerospace Lab*, , No. 11, 2016, pp. 13–pages.

[15] Rose, P. H., "Potential applications of wave machinery to energy and chemical processes," *Proceedings of the 12th International Symposium on Shock Tubes and Waves*, 1979, pp. 3–30.

[16] Kielb, R., Castrogiovanni, A., and Voland, R., "Wave Rotor for Continuous, Vitiate-Free, High-Enthalpy Test Gas," *JANNAF*, 2014.

[17] Wilson, J., and Paxson, D. E., "Jet engine Performance Enhancement Through Use of a Wave-Rotor Topping Cycle," *NASS-TM-4486*, 1993.

[18] Welch, G. E., "Macroscopic balance model for wave rotors," *Journal of Propulsion and Power*, Vol. 13, No. 4, 1997, pp. 508–516.

[19] Banks, J., "Nuclear Thermal Propulsion Systems," , 2023. URL `https://www1.grc.nasa.gov/research-and-engineering/nuclear-thermal-propulsion-systems/`.

[20] Haertling, C., and Hanrahan Jr, R., "Literature review of thermal and radiation performance parameters for high-temperature, uranium dioxide fueled cermet materials," *Journal of nuclear materials*, Vol. 366, No. 3, 2007, pp. 317–335.

[21] Hirschhorn, J., Hilty, F., Tonks, M. R., and Rosales, J., "Review and preliminary investigation into fuel loss from cermets composed of uranium nitride and a molybdenum-tungsten alloy for nuclear thermal propulsion using mesoscale simulations," *JOM*, 2021, pp. 1–16.

[22] Homan, F., Napier, J., and Caldwell, C., "Particle fuels technology for nuclear thermal propulsion," *Conference on Advanced SEI Technologies*, 1991, p. 3457.

[23] Brown, N. R., "A review of in-pile fuel safety tests of TRISO fuel forms and future testing opportunities in non-HTGR applications," *Journal of Nuclear Materials*, Vol. 534, 2020, p. 152139.

[24] Ang, C., Snead, L., and Benensky, K., "Niobium carbide as a technology demonstrator of ultra-high temperature ceramics for fully ceramic microencapsulated fuels," *International Journal of Ceramic Engineering & Science*, Vol. 1, No. 2, 2019, pp. 92–102.

[25] Knight, T., and Anghaie, S., "Advanced carbide fuels for space nuclear thermal propulsion," *37th Joint Propulsion Conference and Exhibit*, 2001, p. 3510.

[26] Matthews, R., Blair, H., Chidester, K., Davidson, K., STARK, W., JR, and STORMS, E., "Carbide fuels for nuclear thermal propulsion," *Conference on Advanced SEI Technologies*, 1991, p. 3455.

[27] Anghaie, S., and Knight, T., "Status of advanced carbide fuels: Past, present, and future," *AIP Conference Proceedings*, Vol. 608, American Institute of Physics, 2002, pp. 852–856.

[28] Williamson, R. L., Hales, J. D., Novascone, S. R., Pastore, G., Gamble, K. A., Spencer, B. W., Jiang, W., Pitts, S. A., Casagranda, A., Schwen, D., et al., "BISON: A flexible code for advanced simulation of the performance of multiple nuclear fuel forms," *Nuclear Technology*, Vol. 207, No. 7, 2021, pp. 954–980.

[29] Sessim, M., and Tonks, M. R., "Multiscale simulations of thermal transport in W-UO2 CERMET Fuel for nuclear thermal propulsion," *Nuclear Technology*, Vol. 207, No. 7, 2021, pp. 1004–1014.

[30] DeHart, M. D., Schunert, S., and Labouré, V. M., "Nuclear thermal propulsion," *Nuclear Reactors: Spacecraft Propulsion, Research Reactors, and Reactor Analysis Topics*, 2022, p. 3.

[31] Gordon, S., and McBride, B. J., "Thermodynamic data to 20,000 K for monatomic gases," Tech. rep., 1999.

[32] McBride, B. J., *Thermodynamic data for fifty reference elements*, National Aeronautics and Space Administration, Glenn Research Center, 2001.

[33] Paxson, D. E., "A general numerical model for Wave Rotor Analysis," National Aeronautics and Space Administration, 1992, p. 1.

[34] Belair, M. L., Sarmiento, C., and Lavelle, T., "Nuclear thermal rocket simulation in NPSS," *49th AIAA/ASME/SAE/ASEE Joint PropulsionConference*, 2013, p. 4001.

[35] Chen, S.-c. S., Veres, J. P., and Fittje, J. E., "Turbopump design and analysis approach for nuclear thermal rockets," *AIP Conference Proceedings*, Vol. 813, American Institute of Physics, 2006, pp. 522–530.

[36] Zagarola, M. V., and McCormick, J. A., "High-capacity turbo-Brayton cryocoolers for space applications," *Cryogenics*, Vol. 46, No. 2-3, 2006, pp. 169–175.

[37] Walter, C. E., "Gas-cooled reactor power systems for space," *4th Symposium on Space Nuclear Power Systems*, 1987, p. 4.

[38] Kiser, J. D., Grady, J. E., Bhatt, R. T., Wiesner, V. L., and Zhu, D., "Overview of CMC (Ceramic Matrix Composite) research at the NASA glenn research center," Tech. rep., 2016.

[39] Read, N., and Shwageraus, E., "Megawatt class space fission power system mass modelling," *Annals of Nuclear Energy*, Vol. 182, 2023, p. 109594.

[40] Morrison, C. G., "Temperature and Power Specific Mass Scaling for Commercial Closed-Cycle Brayton Systems in Space Surface Power and Nuclear Electric Propulsion Applications," *Nuclear Technology*, Vol. 206, No. 8, 2020, pp. 1224–1239.

[41] Harnack, C., Machemer, W., Duchek, M., Grella, E., Nikitaev, D., and Smith, C., "Brayton Cycle Power Conversion Model for MW-Class Nuclear Electric Propulsion Mars Missions," *NETS 2022*, 2022.

[42] Duchek, M. E., Machemer, W., Harnack, C., Clark, M. A., Pensado, A. R., Palomares, K. B., Polzin, K. A., Martin, A., Curran, F., Myers, R., et al., "Key Performance Parameters for MW-Class NEP Elements and their Interfaces," *ASCEND 2022*, 2022, p. 4273.

[43] Grady, J. E., Smith, C. E., Sullivan, R. M., Wiesner, V. L., Hurst, J. B., Arnold, S. M., Zhu, D., Almansour, A. S., Bhatt, R. T., Kalluri, S., et al., "Overview of ceramic matrix composite research at NASA Glenn Research Center," 2017.

[44] Dale, D., and Ruschau, A., "Nasa Hytec CMC Turbine Blade Durability," 2023.

[45] Tomboulian, B. N., "Lightweight, High-temperature radiator for in-space nuclear-electric power and propulsion," 2014.

[46] Dankanich, J. W., and Litchford, R. J., "NASA Envisioned Future Priorities for In-Space Transportation," *International Astronautical Congress (IAC 2022)*, 2022.

[47] Rawlins, S. B., and Thomas, L. D., "Feasibility of Low-Enriched Uranium Fueled Nuclear Thermal Propulsion in the Low-Thrust Region Below 16klbf," *Annals of Nuclear Energy*, Vol. 179, 2022, p. 109368.

[48] Schnitzler, B. G., "Small reactor designs suitable for direct nuclear thermal propulsion: interim report," Tech. rep., Idaho National Lab.(INL), Idaho Falls, ID (United States), 2012.

[49] Sager, P. H., "Radiation shield requirements for manned nuclear propulsion space vehicles," *AIP Conference Proceedings*, Vol. 246, American Institute of Physics, 1992, pp. 1251–1258.

[50] Huynh, C., Hawkins, L., Farahani, A., and McMullen, P., "Design and Development of a Two-Megawatt, High Speed Permanent Magnet Alternator for Shipboard Application," *Naval engineers journal*, Vol. 117, No. 4, 2005, pp. 23–29.

[51] Sivasubramaniam, K., Zhang, T., Lokhandwalla, M., Laskaris, E., Bray, J., Gerstler, B., Shah, M., and Alexander, J., "Development of a high speed HTS generator for airborne applications," *IEEE Transactions on applied superconductivity*, Vol. 19, No. 3, 2009, pp. 1656–1661.

[52] Dyson, R., Rao, D., Duchek, M., Harnack, C., Scheidegger, R., Mason, L., Juhasz, A., Rodriguez, L., Leibach, R., Geng, S., et al., "Nuclear electric propulsion brayton power conversion working fluid considerations," Tech. rep., 2022.

[53] Colozza, A. J., "Small lunar base camp and in situ resource utilization oxygen production facility power system comparison," Tech. rep., 2020.

[54] Heinemann, L., "Analysis and design of a modular, high power converter with high efficiency for electrical power distribution systems," *2002 IEEE 33rd Annual IEEE Power Electronics Specialists Conference. Proceedings (Cat. No. 02CH37289)*, Vol. 2, IEEE, 2002, pp. 713–718.

[55] Swaminathan, N., and Cao, Y., "An overview of high-conversion high-voltage DC–DC converters for electrified aviation power distribution system," *IEEE Transactions on Transportation Electrification*, Vol. 6, No. 4, 2020, pp. 1740–1754.

[56] Jansen, R., De Jesus-Arce, Y., Kascak, P., Dyson, R. W., Woodworth, A., Scheidler, J. J., Edwards, R., Stalcup, E. J., Wilhite, J., Duffy, K. P., et al., "High efficiency megawatt motor conceptual design," *2018 Joint Propulsion Conference*, 2018, p. 4699.

[57] Zhang, D., He, J., Pan, D., Dame, M., and Schutten, M., "Development of megawatt-scale medium-voltage high efficiency high power density power converters for aircraft hybrid-electric propulsion systems," *2018 AIAA/IEEE Electric Aircraft Technologies Symposium (EATS)*, IEEE, 2018, pp. 1–5.

[58] Blandino, J., Gatsonis, N., Cappelli, M., Gallimore, A., Boyd, I., Burton, R., Martinez-Sanchez, M., Batischev, O., Williams, J., Yalin, A. P., Wilbur, P. J., Fisch, N., Raitses, Y., Choueiri, E., Roy, S., and Wang, J., "Overview of electric propulsion research in U.S. academia," *39th AIAA/ASME/SAE/ASEE Joint Propulsion Conference and Exhibit*, 2003.

[59] LaPointe, M., and Mikellides, P., "High power MPD thruster development at the NASA Glenn Research Center," *37th Joint Propulsion Conference and Exhibit*, 2001, p. 3499.

[60] Frisbee, R. H., Hoffman, N. J., and Murray, K. H., "SP-100 Dynamic Power and Lithium-Propellant MPD Nuclear Electric Propulsion Technology Requirements," *AIP Conference Proceedings*, Vol. 301, American Institute of Physics, 1994, pp. 1251–1260.

[61] Gilland, J., McGuire, M., Corle, T., and Clem, M., "Mission Performance of High-Power Electromagnetic Thruster Systems," *AIP Conference Proceedings*, Vol. 813, American Institute of Physics, 2006, pp. 201–208.

[62] Brown, R. D., and Meyers, R. M., "Nuclear Electric Propulsion," *Space Nuclear Propulsion for Human Mars Exploration*, National Academies Press, 2021, pp. 30–54.

[63] Ilin, A. V., Cassady, L. D., Glover, T. W., and Chang Diaz, F. R., "VASIMR® human mission to Mars," *Space, Propulsion & Energy Sciences International Forum*, 2011, pp. 1–12.

[64] Collier-Wright, M. R., La Rosa Betancourt, M. A., Herdrich, G., and Behnke, A., "High-temperature superconductor-based power system architectures as enablers for high power missions," *ASCEND 2021*, 2021, p. 4105.

[65] Landis, G. A., "Analysis of Thermoradiative Thermal Energy Conversion," *APS Eastern Great Lakes Section (EGLS) Fall 2023 Meeting*, 2023.

[66] Hall, L., "Radioisotope Thermoradiative Cell Power Generator," *2023 NASA NIAC Phase I Selection*, 2023. URL `https://www.nasa.gov/general/radioisotope-thermoradiative-cell-power-generator/`.

[67] Borowski, S. K., McCurdy, D., and Packard, T., "Nuclear Thermal Propulsion (NTP): A Proven, Growth Technology for'Fast Transit'Human Missions to Mars," *AIAA SPACE 2013 Conference and Exposition*, 2013, p. 5354.

[68] NASA, "NASA Research Announcement (NRA): Space Technology – Research, Development, Demonstration, and Infusion 2018 (SpaceTech–REDDI–2018), 80HQTR18NOA01," , may 2018.

[69] Bérend, N., Cliquet, E., Ruault, J.-M., and Epenoy, R., "How fast can we go to Mars using high power electric propulsion?" *48th AIAA/ASME/SAE/ASEE Joint Propulsion Conference & Exhibit*, 2012, p. 3889.

[70] Bérend, N., "Optimum design of power-limited propulsion systems with application to fast Earth-to-Mars transfer," *Acta Astronautica*, Vol. 79, 2012, pp. 107–117.

[71] Dankanich, J., Vondra, B., and Ilin, A., "Fast transits to Mars using electric propulsion," *46th AIAA/ASME/SAE/ASEE Joint Propulsion Conference & Exhibit*, 2010, p. 6771.

[72] Williams, J., Senent, J. S., Ocampo, C., Mathur, R., and Davis, E. C., "Overview and software architecture of the copernicus trajectory design and optimization system," *4th International Conference on Astrodynamics Tools and Techniques*, 2010.

[73] Borowski, S. K., Ryan, S. W., Burke, L. M., McCurdy, D. R., Fittje, J. E., and Joyner, C. R., "Robust Exploration and Commercial Missions to the Moon Using NTR LANTR Propulsion and Lunar-Derived Propellants," Tech. rep., 2017.